Laboratori Nazionali di Frascati

LNF-92/085 (P)
4 Novembre 1992

M.R. Pennington:

PREDICTIONS FOR $\gamma\gamma \to \pi\pi$: WHAT PHOTONS AT DAΦNE WILL SEE

Contribution to the DAΦNE Physics Handbook

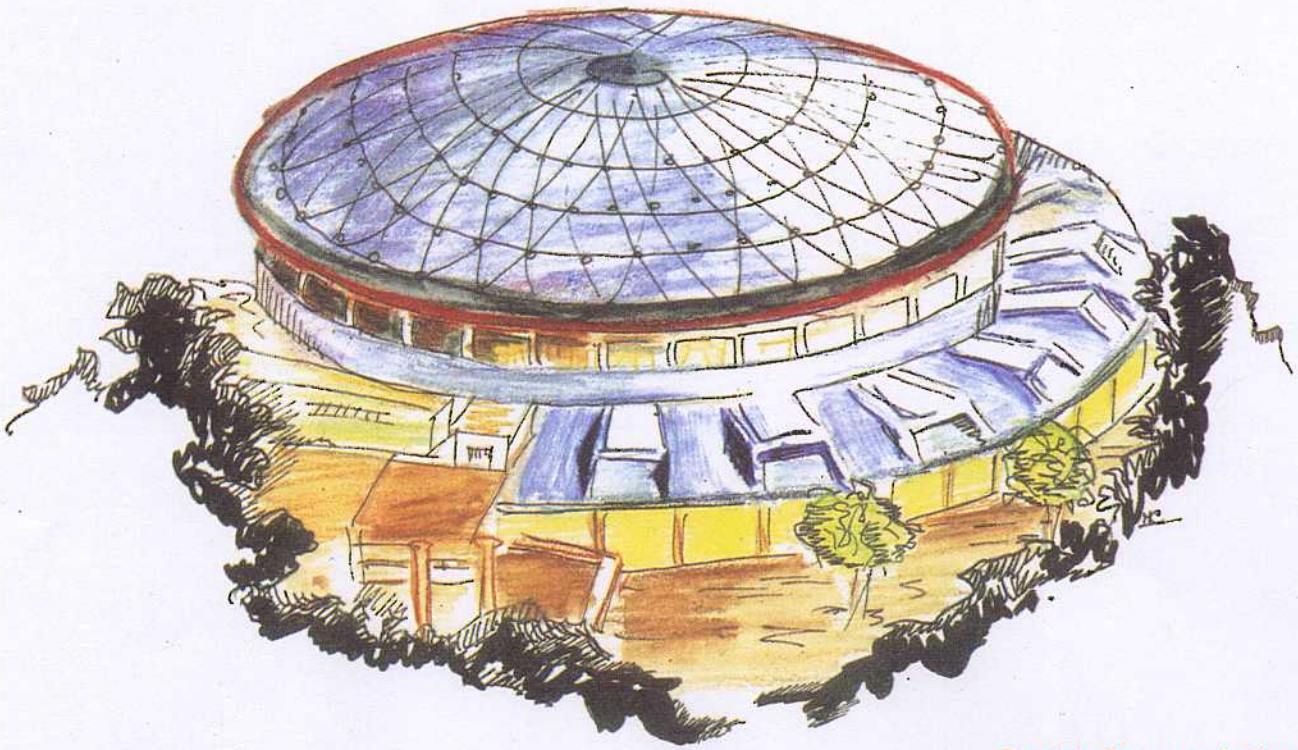

Servizio Documentazione
dei Laboratori Nazionali di Frascati
P.O. Box, 13 - 00044 Frascati (Italy)

INFN - Laboratori Nazionali di Frascati
Servizio Documentazione

LNF-92/085 (P)
4 Novembre 1992

Predictions for $\gamma\gamma \to \pi\pi$: what Photons at DAΦNE will see

M.R. Pennington

Centre for Particle Theory, University of Durham,
Durham DH1 3LE, U.K.

The aim of this article is threefold. Firstly, to discuss briefly why two photon interactions are interesting and then to review what is presently known about them experimentally. Thirdly, to consider how we may predict what DAΦNE may measure. The channel of particular concern is $\gamma\gamma \to \pi^0\pi^0$. The cross-section for this process can be readily calculated in chiral perturbation theory, but the lowest order prediction is not in good agreement with existing data. However, general principles relate this process to other reactions with $\pi\pi$ final states that allow a more general calculational scheme. This predicts cross-sections in much better accord with experiment. The reasons why are analysed in detail. Moreover, we are then able to show how precision measurements of the $\gamma\gamma \to \pi\pi$ cross-section, both for $\pi^+\pi^-$ and $\pi^0\pi^0$, would in turn constrain our knowledge of $\pi\pi$ phases.

1. Introduction : existing data and chiral perturbation theory

A beautiful feature of an e^+e^- machine is its ability to study two photon processes. The cross-section for $e^+e^- \to e^+e^-X$ is dominated by the exchange of two *almost real* photons, so that one can really extract information on $\gamma\gamma \to X$, where X is hadronic, as seen in Fig. 1 [1].

In the low energy region, such information not only sheds light on the structure of hadrons, but can provide insight into the workings of hadron dynamics. At low momenta, $\pi\pi$, having the lowest threshold energy, is naturally the most abundantly produced hadronic final state. What this can teach us can be seen by considering $\gamma\gamma \to \pi\pi$ from the t-channel point of view, Fig. 1b, where we think of the photon scattering off a pion. At low energies, the photon, having long wavelength sees the whole hadron and couples to its electric charge. Thus, the photon sees the charged pions, but not the neutral, so the cross-section for $\gamma\gamma \to \pi^+\pi^-$ is large compared to that for $\pi^0\pi^0$ production, see Fig. 2 [2,3]. However, as the energy of the photon increases and its wavelength shortens, it recognises that the pions, whether charged or neutral, are made of the same charged constituents, namely quarks, and causes these to resonate.

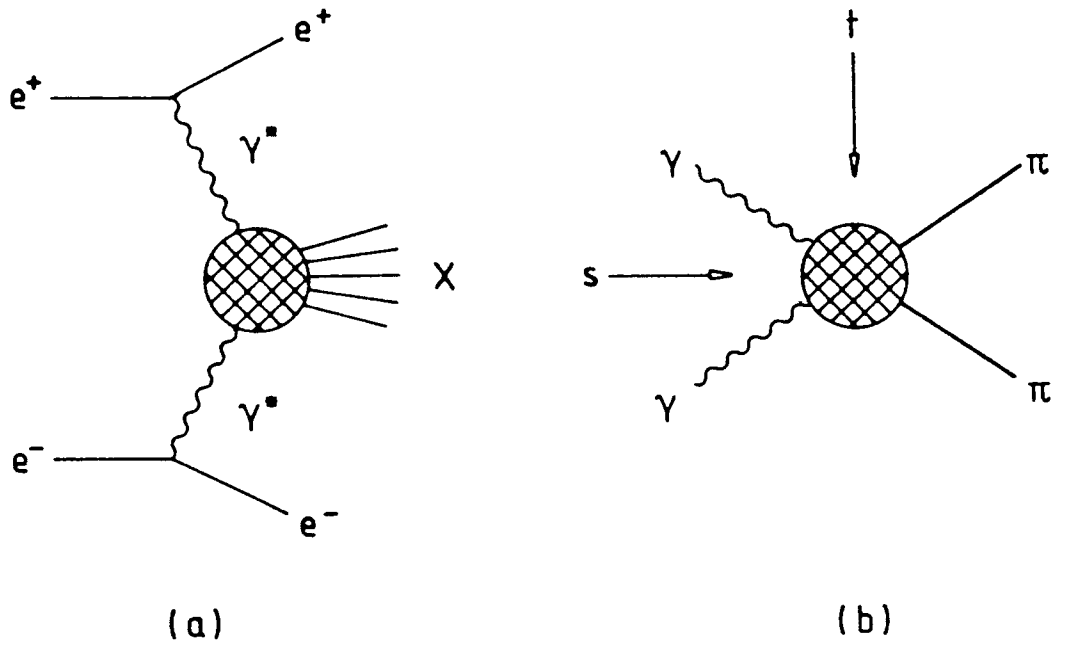

Fig. 1 : (a) $e^+e^- \to e^+e^-X$ when dominated by two photon exchange ;
(b) $\gamma\gamma \to \pi\pi$ showing the s and t-channels.

Consequently, the cross-section for both $\gamma\gamma \to \pi^+\pi^-$ and $\pi^0\pi^0$ are dominated by the well-known $q\bar{q}$ tensor meson, the $f_2(1270)$ resonance. With complete data, these cross-sections can be separated into individual spin components [4] and the couplings of not just the tensor $f_2(1270)$, but also those of any underlying scalars, can be extracted [5] — scalar and tensor states are readily produced by two real photons with no need for any relative orbital angular momentum. The extraction of such $\gamma\gamma$ couplings is especially useful since it can teach us about the make-up of these hadronic states. This is because the coupling is proportional to the fourth power of the charges that the photons see and to the probability of the annihilation of the hadron's constituents. Thus for scalar states made of $q\bar{q}$, $K\overline{K}/qq\overline{qq}$ or gg, we may expect quite different couplings [6,7].

Here, we will concentrate on what we can learn about hadron dynamics at low energies towards threshold. This is not only valuable for anchoring the *Amplitude Analysis* needed to extract resonance couplings, but, as we shall see, may aid our understanding of Chiral Dynamics. First we shall review existing data.

The earliest results on charged final states are from four sets of experiments : DELCO [8] and TPC/$\gamma\gamma$ [9] at SLAC, PLUTO [10] at PETRA and DM1/2 [11] at DCI-Orsay. The first three have most data in the f_2-region, but PLUTO were able

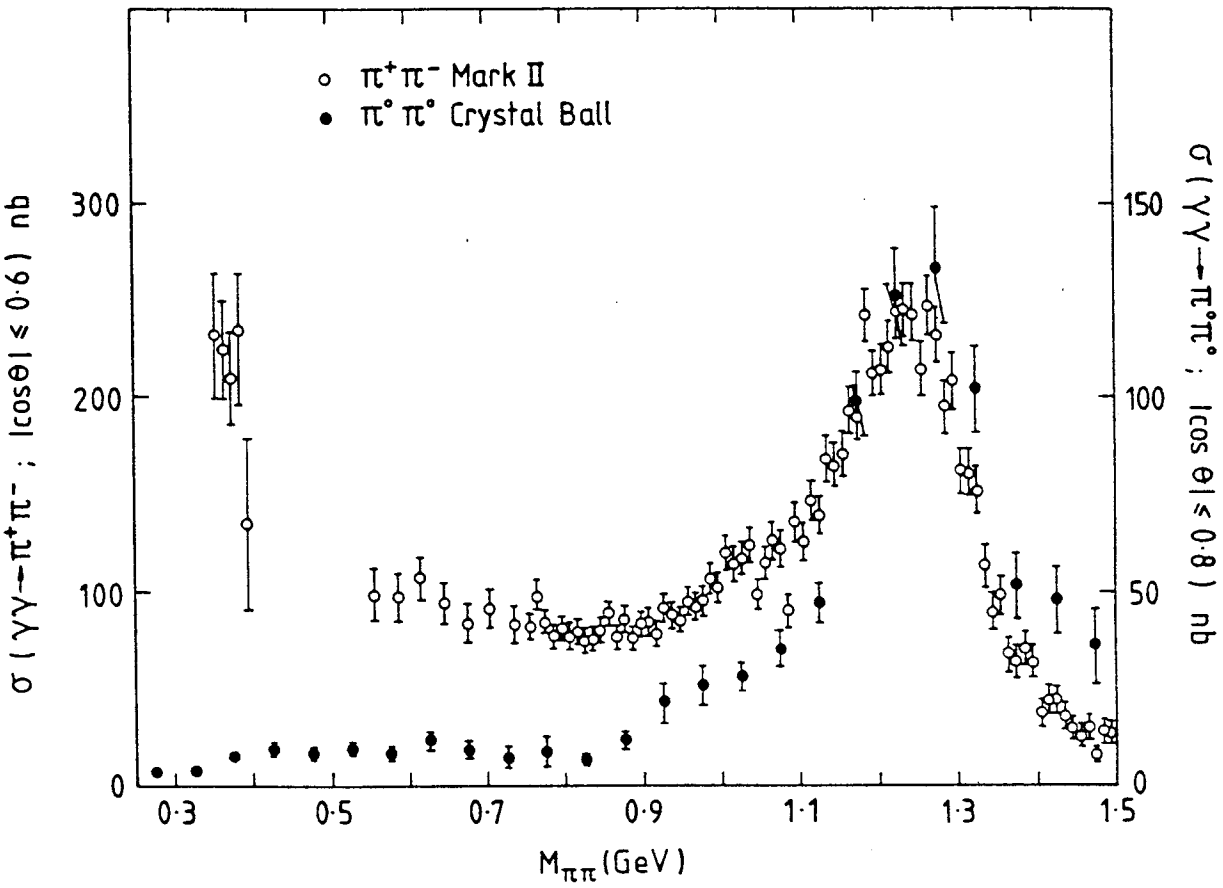

Fig. 2 : $\gamma\gamma \rightarrow \pi^+\pi^-$ cross-section (open circles, left hand scale) for $|\cos\theta| \leq 0.6$ from Mark II [2] and the $\gamma\gamma \rightarrow \pi^0\pi^0$ cross-section (solid circles, right hand scale) for $|\cos\theta| \leq 0.8$ from Crystal Ball [3] as a function of $\pi\pi$ invariant mass. These two would be equal if the I=0 components dominate and if the unobserved angular region contributes negligibly.

to measure a cross-section (with large errors) near threshold. This cross-section is somewhat bigger than naive expectations from the Born model we discuss in section 2. This PLUTO result (Fig. 3a) seemed to be confirmed by the Orsay experiments, which suggested a cross-section twice as large as the Born estimate. In fact, the DM1/2 experiments never presented cross-sections, but rather a comparison of their event distributions with the Born estimate passed through a Monte Carlo of their detector (Fig. 3b).

However, more recently, Mark II at PEP have measured the $\pi^+\pi^-$ cross-section, with much higher statistics (Fig. 2) revealing a low energy cross-section much smaller than DM1/2 and indicated by the central values from PLUTO. That the earlier low statistics

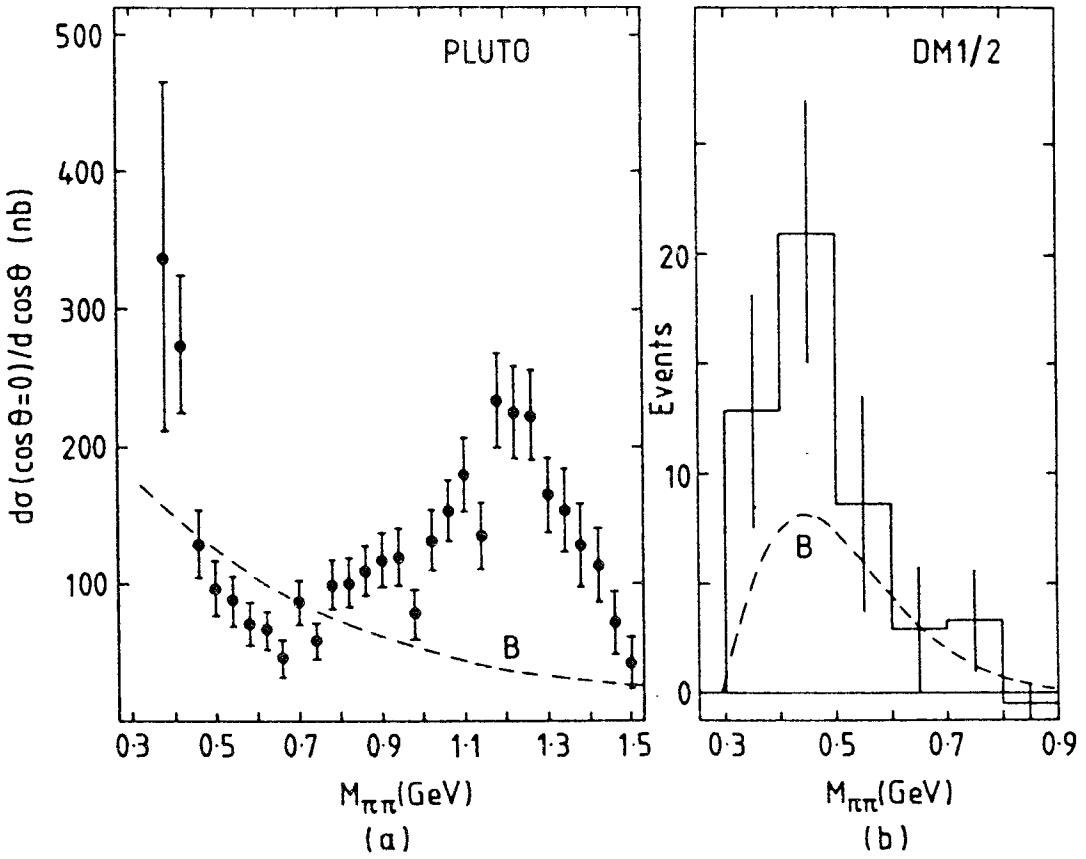

Fig. 3 : (a) Experimental results on $\gamma\gamma \to \pi^+\pi^-$ cross-section from the PLUTO group [10] $d\sigma/d\cos\theta$ for $|\cos\theta| \leq 0.2$ as a function of $M_{\pi\pi}$. The dashed curve, B, is the Born cross-section — sect. 2 ;
(b) Experimental spectrum on $\gamma\gamma \to \pi^+\pi^-$ as a function of $M_{\pi\pi}$ from the combined results from DM1 ($|\cos\theta| \leq 0.64$) and DM2 ($|\cos\theta| \leq 0.71$) [11] again compared with the reported Born spectrum, B.

results may have sizeable systematic uncertainties is readily seen from the way DM1/2 separate their $\pi^+\pi^-$ events. Their detector sees charged particle final states, which at low energies can only be e^+e^-, $\mu^+\mu^-$ and $\pi^+\pi^-$. The lepton pair cross-sections are, of course, calculable in QED and the $\pi^+\pi^-$ component is merely identified as the surplus of charged pairs above these calculable backgrounds. As seen from Fig. 4, small statistics make this separation far from exact.

The main $\pi^0\pi^0$ detector to date is Crystal Ball, which, while running at SPEAR, only studied the f_2-region of $\pi\pi$ production [12]. On its removal and reconstruction at DORIS, Crystal Ball took much higher statistics data [3], which extended these studies right down to threshold (Fig. 2). Indeed, these Crystal Ball results provide the only normalized low energy $\pi^0\pi^0$ cross-section. Above 800 MeV, there are now twice as much data, which within a 15% normalization uncertainty [13], are in agreement with

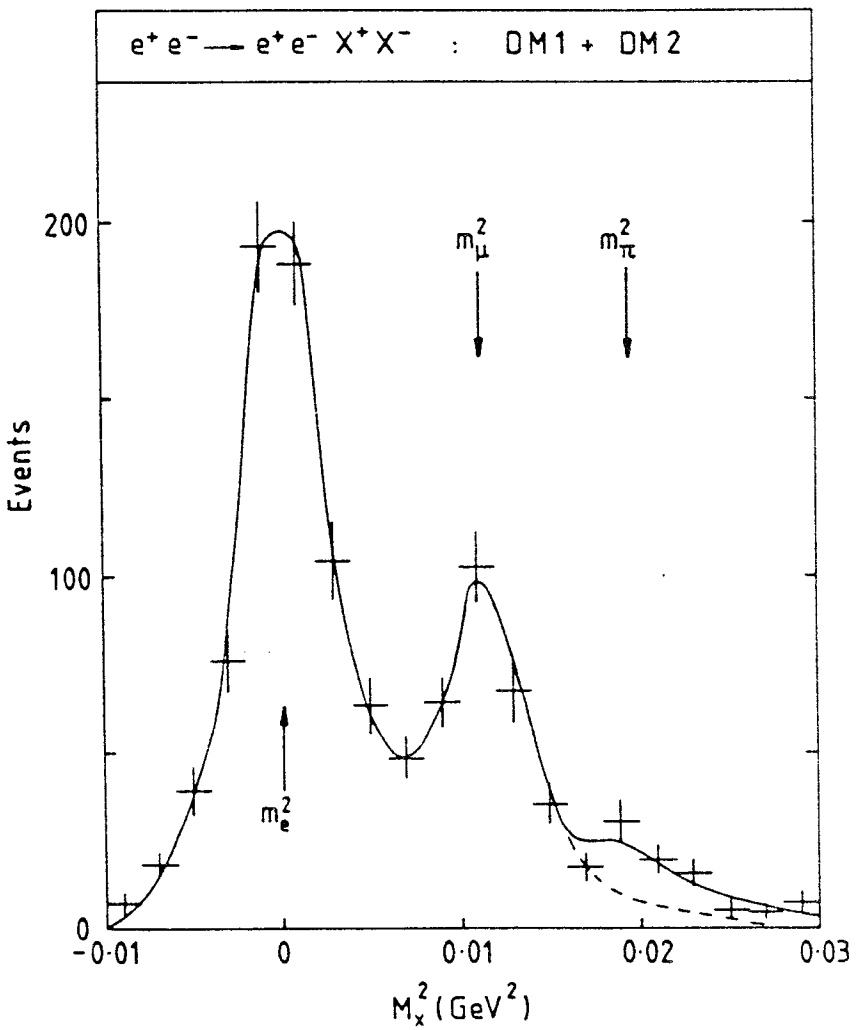

Fig. 4 : The charged pair spectrum as a function of the mass squared of the pair from the combined DM1 and DM2 experiments [11]. The solid line shows the best fit including electron, muon and pion production. The dashed line is the fit without the pion contribution.

the older data. In addition there are results on $\pi^0\pi^0$ from threshold to 2500 MeV from JADE [14], but these are merely raw events uncorrected for acceptance and efficiency. These we shall discuss later.

The pion, by the far the lightest hadron, has long been regarded as the (massless) Goldstone boson associated with the spontaneous breakdown of chiral symmetry. Moreover, its emission in any process is controlled by the divergence of the axial vector current. In a world of massless pions, this current would be conserved. This leads to low energy theorems that require the amplitude for the emission of a pion to be equal to its Born amplitude, when the pion has zero momentum [15]. Such consequences of a conserved current will be met again in sect. 2 in the context of QED, so essential for photon reactions. In a process, like $\pi\pi \to \pi\pi$, where G-parity allows no Born amplitude,

such consistency conditions impose a zero at threshold — the Adler zero. Since the real world is very close to the massless pion one, this zero appears near threshold for physical pions. This smooth extrapolation is embodied in the folklore of the Partial Conservation of the Axial Current (PCAC), where the extrapolation parameter $m_\pi^2/16\pi^2 f_\pi^2$ is very much less than 1 (f_π being the pion decay constant). Remarkably such zeros are very much a feature of the real world explored by experiment. Consequently, while pions obviously interact strongly, the presence of such zeros mean that their interactions are surprisingly weak near threshold and so one can imagine a perturbative expansion in powers of $q^2/16\pi^2 f_\pi^2$, where q is the pion 4-momentum [16]. This idea has been systematically developed in the extensive technology of Chiral Perturbation Theory by Gasser and Leutwyler [17]. This expansion is underpinned by a most general Lagrangian, but like many an effective theory, it is not renormalizable in terms of a finite number of constants. Thus the perturbative expansion acquires new parameters at every order, which require an increasingly large number of experimental facts to fix.

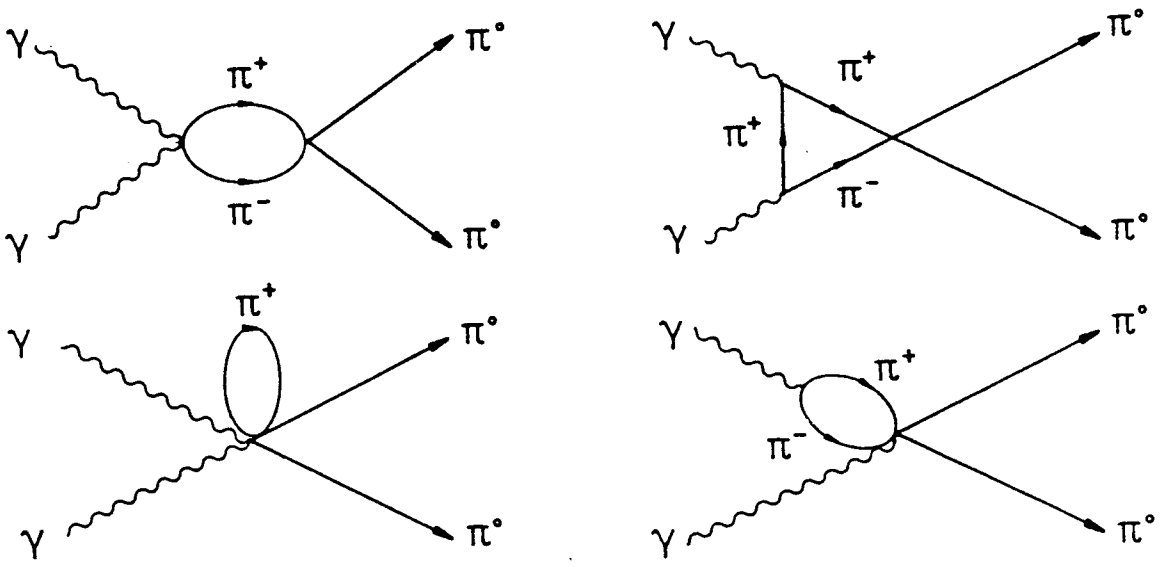

Fig. 5 : Lowest order contributions to $\gamma\gamma \to \pi^0\pi^0$ in Chiral Perturbation Theory [18,19].

However, the reaction $\gamma\gamma \to \pi^0\pi^0$ is of particular interest because it can be exactly predicted in Chiral Perturbation Theory, at least at lowest order. The one loop contributions shown in Fig. 5 have been computed by both Bijnens and Cornet [18] and by Donoghue, Holstein and Lin [19]. These graphs have cancelling divergences and as a consequence the predicted cross-section is, to this order, finite without renormalization. In Fig. 6, this prediction is compared with the Crystal Ball data [3] (Fig. 2). The

Crystal Ball experiment only covers $|\cos\theta| \leq 0.8$ and the data have been scaled to the full angular range by simply multiplying by 1.25. This is justified, as we discuss in detail in sect. 2, since the $\pi^0\pi^0$ cross-section is overwhelmingly S-wave in this energy region. Clearly, Chiral Perturbation Theory predicts a cross-section of the same order of magnitude, but the shape is quite different. The data rise from threshold and are then essentially flat for hundreds of MeV (Fig. 2), while Chiral Perturbation Theory at lowest order gives an almost linearly increasing prediction. Reassuringly, this crosses the data around 500 MeV, which is still where we might expect low orders in Chiral Perturbation Theory to apply. Of course, the prediction beyond one loop is expected to be modified at higher energies. Bijnens, Dawson and Valencia [20] have estimated this by including the effect of quark loops and find that while near threshold these are negligible, above 400 MeV they flatten the cross-section, Fig. 6. Similar effects are generated by other higher order contributions, like vector mesons, Fig 6. These components have been computed by Ko [21] and more recently by Babusci and Bellucci [22] for the DAΦNE workshop. The implications of these studies is that higher orders must be large above 400 MeV, but near threshold a definite prediction is made that disagrees with existing experimental results from Crystal Ball by at least a factor of 2.

We must therefore conclude that either

(i) the Crystal Ball data, or

(ii) the predictions of Chiral Perturbation Theory,

or both of these, are not correct near threshold.

As already mentioned $\pi^0\pi^0$ data have been taken by the JADE group [14] during the final runs at PETRA, with comparable statistics to the first Crystal Ball results at DORIS. The spectrum, Fig. 7c, has a somewhat different shape to the Crystal Ball cross-section, Fig. 7a, and has been used to suggest, by normalizing the JADE events in an *ad hoc* way to the Crystal Ball cross-section on the $f_2(1270)$, that the Crystal Ball results are inaccurate at low energies by factors of 2 or 3 [22,23]. This is, of course, to misjudge the critical importance of the angular and energy efficiency corrections that **have been** applied to the Crystal Ball data, but **not** to those of JADE. In Fig. 7b, the Crystal Ball spectrum, before these corrections, is displayed. One sees immediately how such raw spectra can not be used as a guide to the relation of the cross-section at 1300 MeV to that at 300 MeV. Consequently, with no man-power available to correct the JADE events, we have to live with the fact that the Crystal Ball experiment is the only one to provide a normalized cross-section.

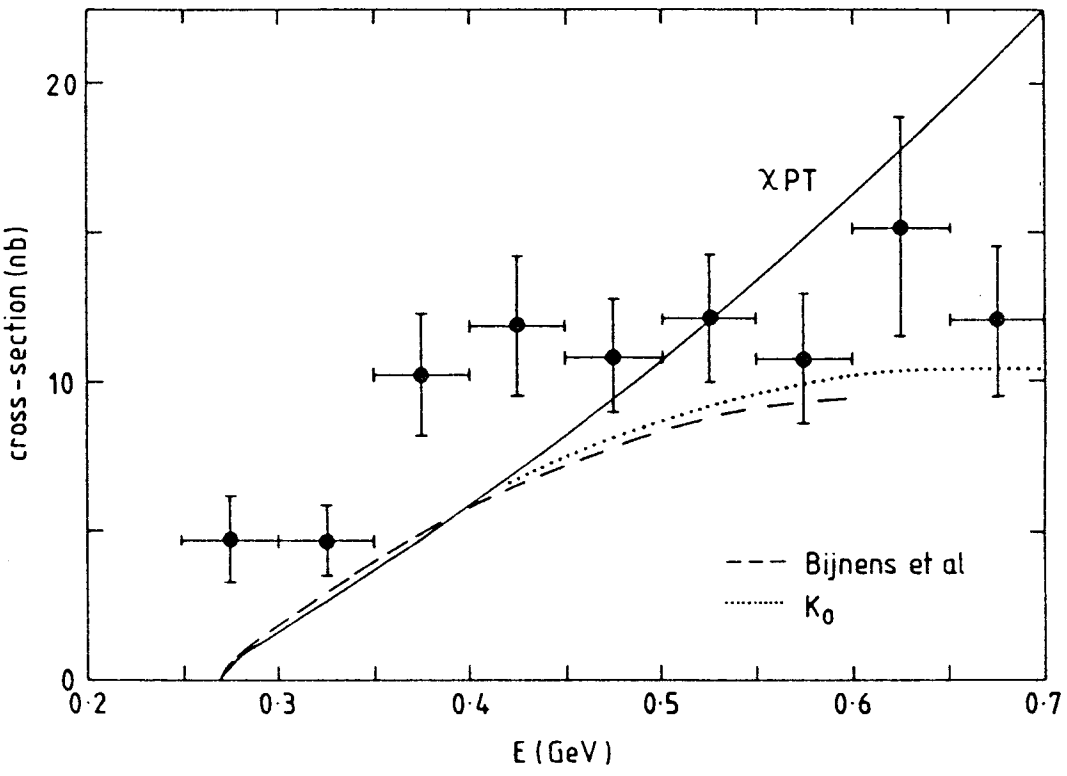

Fig. 6 : Integrated cross-section for $\gamma\gamma \to \pi^0\pi^0$ as a function of the $\pi\pi$ invariant mass, $E = \sqrt{s}$. The data are from Crystal Ball [3], as in Fig. 2, scaled to the full angular range by a factor of 1.25. The line marked χPT is the prediction of lowest order Chiral Perturbation Theory [18,19]. The dashed line illustrates the effect of adding quark loop contributions to the Chiral Perturbation Theory result as calculated by Bijnens et al. [20], while including vector mesons instead gives the dotted line computed by Ko [21].

To attempt to resolve whether either of low orders in Chiral Perturbation Theory or the Crystal Ball data are correct, we need an independent way of modelling the amplitude for $\gamma\gamma \to \pi\pi$ and this is what we are going to discuss next. Fortunately, there are a number of general properties any description of this process must satisfy and these allow us to predict the low energy cross-sections from first principles. We will see, for instance, that the prediction of Chiral Perturbation Theory that the cross-section for $\gamma\gamma \to \pi^0\pi^0$ is proportional to that for $\pi^+\pi^- \to \pi^0\pi^0$ [19] only holds in rather special circumstances.

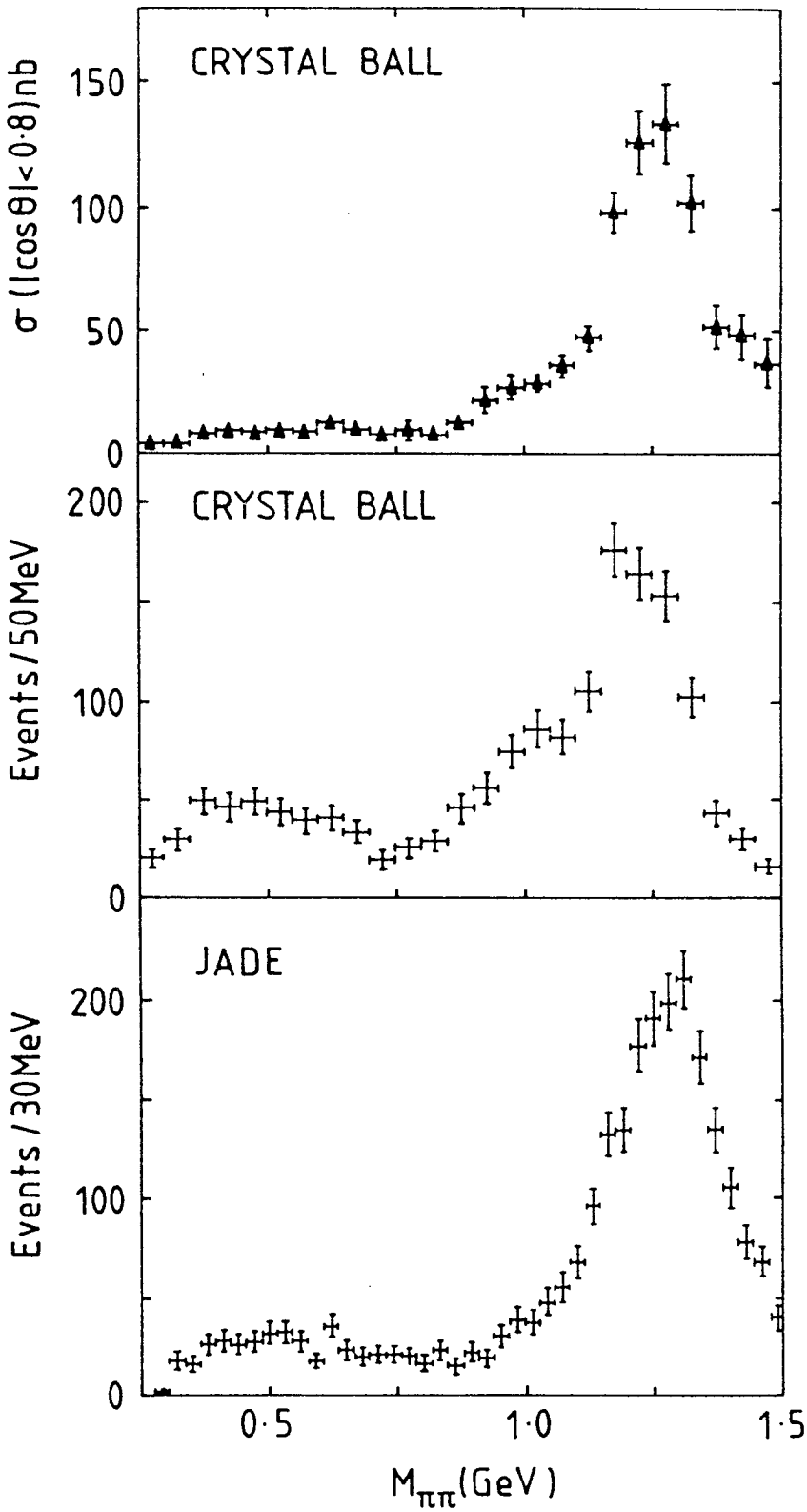

Fig. 7 : Experimental results on $\gamma\gamma \to \pi^0\pi^0$ as a function of the $\pi\pi$ invariant mass, $M_{\pi\pi}$.
(a) Normalized cross-section from Crystal Ball [3] for $|\cos\theta| \leq 0.8$;
(b) Raw spectrum from Crystal Ball from which (a) has been deduced by correcting for angular acceptance and efficiency ;
(c) Raw spectrum from JADE [14].

2. $\gamma\gamma \to \pi\pi$ from general principles and PCAC

We consider dipion production by real photons. The Mandelstam variables are defined as in Fig. 1b, so that $s = M_{\pi\pi}^2$. As is well-known [1,24,4], the amplitude for this process has two independent helicity components $\mathcal{M}_{++}$, $\mathcal{M}_{+-}$, which contribute incoherently to the unpolarized cross-section :

$$\frac{d\sigma}{d\Omega} = \frac{\beta}{128\pi^2 s}\left[\,|\,\mathcal{M}_{++}\,|^2 + |\,\mathcal{M}_{+-}\,|^2\right] \tag{1}$$

where $\beta = \sqrt{1-4m_\pi^2/s}$. The helicity amplitudes $\mathcal{M}_{++}$ and $\mathcal{M}_{+-}$ correspond to photon helicity differences of $\lambda = 0, 2$ respectively. These have partial wave expansions involving even $J \geq \lambda$:

$$\begin{aligned}\mathcal{M}_{++}(s,\theta,\phi) &= e^2\sqrt{16\pi}\sum_{J\geq 0}\mathcal{F}_{J0}(s)\,Y_{J0}(\theta,\phi)\\ \mathcal{M}_{+-}(s,\theta,\phi) &= e^2\sqrt{16\pi}\sum_{J\geq 2}\mathcal{F}_{J2}(s)\,Y_{J2}(\theta,\phi)\end{aligned} \tag{2}$$

where the factor of $e^2\sqrt{16\pi}$ has been taken out for later convenience. With this normalization the integrated cross-section is

$$\sigma = 2\pi\alpha^2\frac{\beta}{s}\sum_{J\geq\lambda}|\,\mathcal{F}_{J\lambda}\,|^2 \tag{3}.$$

Like all reactions $\gamma\gamma \to \pi\pi$ must have a description that is relativistic and causal and conserves probability. This means that the processes $\gamma\gamma \to \pi\pi$ and $\gamma\pi \to \gamma\pi$ are represented everywhere in the Mandelstam plane, Fig. 8, by an analytic amplitude, we denote generically by $\mathcal{F}(s,t)$. † Moreover, since the process involves photons, this amplitude is constrained by current conservation and it is with this property that we begin. The fact that the photon at threshold in $\gamma\pi \to \gamma\pi$ sees the whole hadron and couples to its electric charge gives a low energy theorem [25]. Low's theorem states that the amplitude $\mathcal{F}$ for $\gamma\pi \to \gamma\pi$ tends to its Born amplitude, $\mathcal{B}$, as $s \to 0$, $t, u \to m_\pi^2$:

$$\mathcal{F}(s,t) \to \mathcal{B}(s,t) \qquad \text{as } s \to 0, \quad t \to m_\pi^2 \tag{4}.$$

For charged pions, the Born amplitude is given by the graphs of Fig. 9. This involves the simplest gauge invariant contributions to $\mathcal{F}$, namely one-pion-exchange in the t-channel,

† this can be the s-channel helicity amplitudes $\mathcal{M}_{+\pm}$, or the invariant amplitudes.

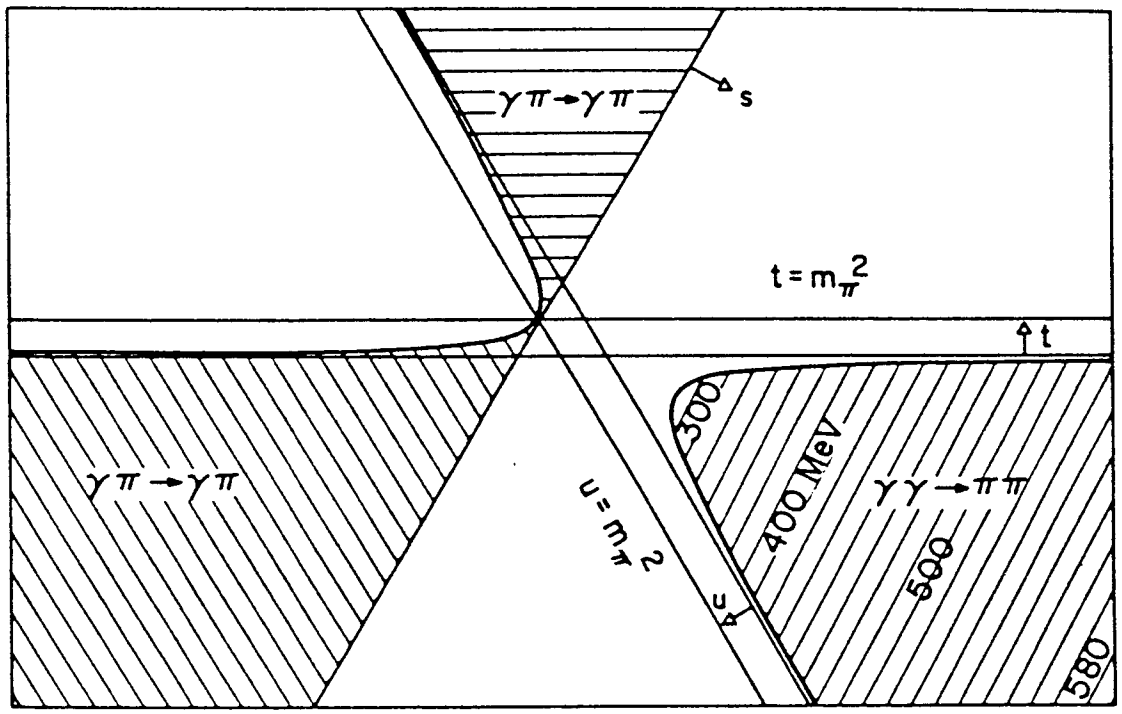

Fig. 8 : Mandelstam plane showing the three related physical regions, s-channel : $\gamma\gamma \to \pi\pi$, t & u-channels : $\gamma\pi \to \gamma\pi$.

one-pion-exchange in the u-channel plus a seagull graph to ensure gauge invariance. This amplitude we denote by $\mathcal{B}_\pi$. For neutral pions, the Born amplitude is, of course, zero.

Though the theorem states that the $\gamma\pi \to \gamma\pi$ amplitude equals the Born result at just one point in the Mandelstam plane, it, in fact, approaches this limit smoothly along any line at fixed scattering angle [26]. Thus away from $\gamma\pi$ threshold, we can write the amplitude as $\mathcal{F} = \mathcal{B} + \mathcal{L}$, where $\mathcal{L}$, the left-over part, vanishes as $s \to 0$, $t, u \to m_\pi^2$. Now $\mathcal{L}$ will receive contributions from other t, u-channel exchanges, like ρ, ω exchange. Let us consider the effect of these poles by looking at the Mandelstam plane, Fig. 8. Drawn to scale we see the three physical regions related by crossing : $\gamma\pi \to \gamma\pi$ in the t, u-channels and $\gamma\gamma \to \pi\pi$ in the s-channel. We see the pion poles very close to these physical regions passing close to both the forward and backward directions. The only point at which they actually cross the physical region is at $\gamma\pi$ threshold. It is here that Low's theorem applies — the amplitude is equal to the Born contribution. In comparison, the vector meson exchange poles are far from the $\gamma\gamma \to \pi\pi$ physical region at low energies and, as these exchanges have couplings no larger than pions have, we expect them to make a rather small perturbation to the charged pion amplitude. Thus when we are near $\pi^+\pi^-$ threshold, the pion poles are so very close and these other exchanges so far away, that we expect the Born amplitude, $\mathcal{B}_\pi$, to continue to control the

$\gamma\gamma \to \pi^+\pi^-$ amplitude. However, at higher energies, like 5-600 MeV, though the pion poles are still very near the forward and backward directions, the vector meson poles are no longer disproportionately far from the middle of the scattering region and so they start to have an increasingly important role. Thus only in the near threshold region do we expect the known Born amplitude to fix the $\gamma\gamma \to \pi^+\pi^-$ cross-section absolutely. The closeness of the pion poles has yet another effect on the $\gamma\gamma \to \pi\pi$ process. Crossed-channel poles are built from an infinite number of direct-channel partial waves. Thus the s-channel $\gamma\gamma \to \pi^+\pi^-$ amplitude must have sizeable higher partial waves. So while the S-wave always controls the near threshold behaviour, D-waves very rapidly become important, being only suppressed by a factor of $(1 - 4m_\pi^2/s)$. Thus, the angular distribution for $\gamma\gamma \to \pi^+\pi^-$ scattering is not expected to be flat above 500 MeV or so. Indeed, this means that acceptance correcting the observed event distribution is highly sensitive to the near forward and backward regions not detected in two photon experiments. In contrast, the lack of a Born component for $\pi^0\pi^0$ production and the fact that near threshold its crossed-channel exchanges are far away means the $\pi^0\pi^0$ angular distribution must be much flatter and hence S-wave dominated [27,5].

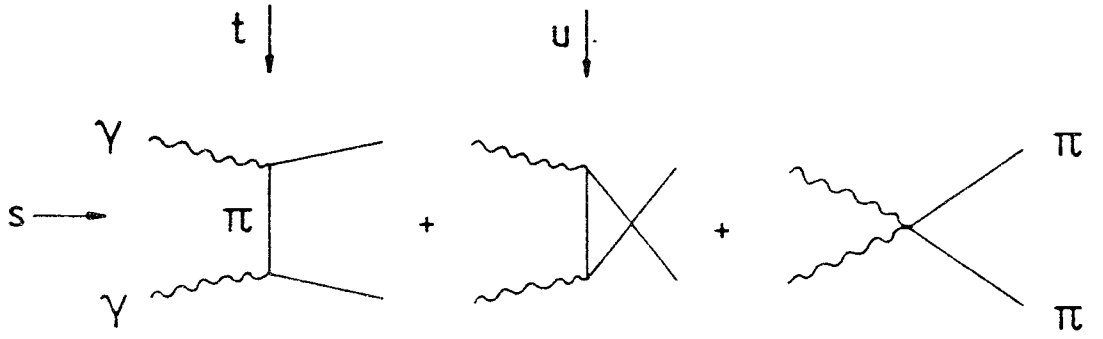

Fig. 9 : QED Born amplitude for $\gamma\gamma \to \pi^+\pi^-$ is the sum of these three Feynman diagrams.

In hadronic processes, it is a feature of nature, readily explained by the quark model, that $I = 2$ cross-sections are much smaller than those with $I = 0$. However, here in $\gamma\gamma \to \pi\pi$, because of the importance of the pion exchange contributions, the amplitude with $I = 2$ for the final state pions is just as important as that for $I = 0$. Indeed, the large $\pi^+\pi^-$ cross-section results from a constructive interference of the $I = 0, 2$ amplitudes, while the very small $\pi^0\pi^0$ cross-section comes from their destructive interference. Thus an *Amplitude Analysis* requires the measurements of both the $\pi^+\pi^-$ and $\pi^0\pi^0$ distributions to make the separation of $I = 0, 2$ components at all feasible [4,5,27].

To proceed, we need to be more precise about the meaning of the non-pion exchange part of the amplitude $\mathcal{F}$. In a relativistic, causal description, we can quite generally separate it into two parts. One we continue to call $\mathcal{L}$, which is generated by all t, u-channel exchanges other than the pion. The other, we call $\mathcal{R}$, is generated by final state interactions. These make the whole amplitude $\mathcal{F} = \mathcal{B} + \mathcal{L} + \mathcal{R}$ complex. To see how we can determine these pieces, it is convenient to separate our amplitude into components with definite isospin, spin and helicity in the $\gamma\gamma$ centre-of-mass, as given in Eq. (2). To avoid a proliferation of indices that may obscure the discussion, we continue to denote the partial wave components of our amplitude and its contributions by $\mathcal{F}$, $\mathcal{B}$, $\mathcal{L}$ and $\mathcal{R}$, though now these will just be a function of the single variable s. In a relativistic causal description, each such spin amplitude is analytic in the cut s-plane, with a left hand cut for $s \leq 0$ and a right hand cut for $s \geq 4m_\pi^2$. The nearby part of the left hand cut, starting at $s = 0$ is associated with pion exchange, while $\mathcal{L}$ has the left hand cut expected to be associated with ρ, ω and all other exchanges, starting at $s = -(m_V^2 - m_\pi^2)^2/m_V^2$ (where m_V is the mass of the exchange). Consequently, its S-wave, $\mathcal{L}$, would then be $s^2/(s+m_V^2)^2$: 1 when compared to that of the Born amplitude $\mathcal{B}_\pi$. Experiment will check if this is so. Final state interactions give $\mathcal{R}$ a right hand cut. Thus quite generally we can write

$$\begin{aligned} \mathcal{F}(s) &= \mathcal{H}(s) + \mathcal{R}(s) \\ &= \mathcal{B}(s) + \mathcal{L}(s) + \mathcal{R}(s) \end{aligned} \tag{5}$$

where $\mathcal{H}$ contains the complete left hand cut of $\mathcal{F}$ and $\mathcal{R}$ the right hand cut and Low's theorem, Eq. (4), is satisfied by

$$\mathcal{L}(s) \to 0\,, \qquad \mathcal{R}(s) \to 0 \qquad \text{as} \quad s \to 0 \tag{6}$$

— indeed they vanish at least linearly with s [26].

Let us note that even if there were no other left hand cut contributions than given by one pion exchange (i.e. $\mathcal{L} = 0$), final state interactions would make the $\pi^0\pi^0$ amplitude non-zero, since $\gamma\gamma \to \pi^+\pi^- \to \pi^0\pi^0$. If the first step is given by the Born amplitude, one may imagine calculating this process, as we shall describe below, and obtaining a first estimate of the $\pi^0\pi^0$ cross-section. We shall see it will give an answer in the right ball-park of tens of nanobarns.

Final state interactions are indeed calculable at low energies because pions scatter universally regardless of how they are produced. This is a consequence of the conservation of probability. The fact that one cannot get more out in a scattering process

than one puts in requires that the S-matrix be unitary. The consequences of this are most readily expressed in terms of amplitudes with definite spin and isospin — hence our introduction of these.

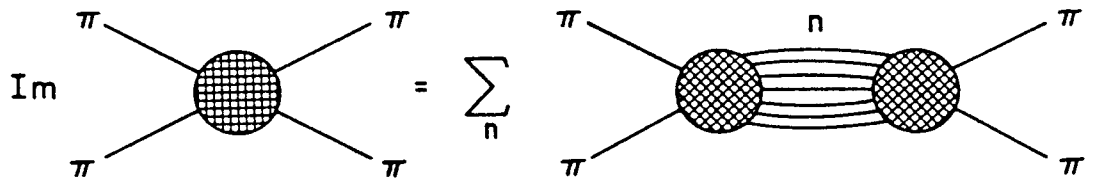

Fig. 10 : Unitarity condition for $\pi\pi \to \pi\pi$ amplitudes with definite I and J.

First, unitarity says that for a hadronic reaction, like $\pi\pi \to \pi\pi$, the imaginary part of each of its partial wave amplitudes, $\mathcal{T}$, is given by the relation of Fig. 10, where one has to sum over all intermediate states, n, that are kinematically allowed. Now, in the low energy region, there is only one intermediate state possible, namely $\pi\pi$ itself. There the relation simplifies to

$$\mathrm{Im}\,\mathcal{T}(\pi\pi \to \pi\pi) \;= |\,\mathcal{T}(\pi\pi \to \pi\pi)\,|^2 \tag{7}$$

which is satisfied by the well-known phase-shift relation

$$\mathcal{T}(\pi\pi \to \pi\pi) \;=\; \sin\delta\, e^{i\delta} \tag{8}.$$

The non-linearity of Eq. (7) means, as seen in Eq. (8), that measuring the modulus of the $\pi\pi$ elastic amplitude tells us its phase and measuring its phase tells us its modulus. While strictly speaking, elastic unitarity applies up to 4π threshold, in practice multipion channels are known to be quite unimportant until we reach $\rho\rho$, $\omega\omega$ thresholds, so $K\overline{K}$ is the first strongly coupled inelastic channel. Consequently, Eqs. (7,8) hold up to almost 1 GeV. Above that energy the unitarity relation becomes more complicated, but nevertheless just as constraining. Thus from measurements of the $\pi\pi \to \pi\pi$ and $\pi\pi \to K\overline{K}$ differential cross-sections one can in turn determine the corresponding phase-shifts for each partial-wave amplitude. We shall see shortly why these are important for $\gamma\gamma$ physics. The $I = 0$ S-wave phase indicates two dynamical features : the broad ϵ and the narrow S^* close to $K\overline{K}$ threshold. The $I = 0$ D-wave is controlled by the $f_2(1270)$.

Now the same unitarity conditions require that in the low energy region the amplitude $\mathcal{F}$ for $\gamma\gamma \to \pi\pi$ satisfies a similar constraint, Fig. 11 :

$$\mathrm{Im}\,\mathcal{F}(\gamma\gamma \to \pi\pi) = \mathcal{F}(\gamma\gamma \to \pi\pi)^* \mathcal{T}(\pi\pi \to \pi\pi) \qquad (9),$$

again for amplitudes with definite I, J. Eq. (9) ensures that any resonance in $\pi\pi \to \pi\pi$ also appears in $\gamma\gamma \to \pi\pi$ and vice versa, as they must. This condition, which is linear in $\mathcal{F}$ puts no constraint on the strength of $\gamma\gamma \to \pi\pi$ scattering, but it does require that if $\mathcal{F}$ has phase $\phi(s)$, where $\mathcal{F}(s) = |\,\mathcal{F}(s)\,|\, e^{i\phi(s)}$, then Eqs. (8,7) imply Watson's final state interaction theorem [28] :

$$\phi(s) = \delta(s) \qquad (10)$$

for each spin and isospin. We are, in fact, allowed to add multiples of π to either side of Eq. (10), but the behaviour at $\pi\pi$ threshold ensures these are absent, as $\phi(s)$, $\delta(s) \to 0$ as $s \to 4m_\pi^2$. This theorem ensures that the two pions scatter in the same way however they are produced. Above inelastic threshold, again unitarity is still powerful, it says that all $\pi\pi$ amplitudes have the same right hand cut structure.

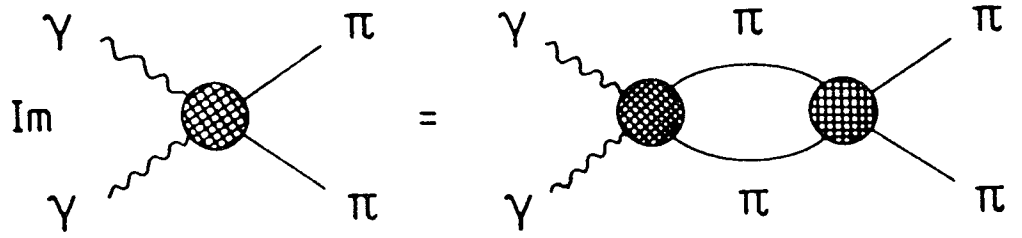

Fig. 11 : Unitarity constraint for $\gamma\gamma \to \pi\pi$ in the energy region below the first inelastic threshold, effectively 1 GeV.

Thus, we have learnt that up to 1 GeV or so, the universal scattering of final state pions means we know the phase of each $\gamma\gamma \to \pi\pi$ partial wave amplitude, $\mathcal{F}$, from purely hadronic data. To implement this knowledge, let us assume we know the phase $\phi(s)$ of $\mathcal{F}$ for all $s > 4m_\pi^2$. Then we can construct an analytic function, $\Omega(s)$, the Omnès function [29,4] that has exactly this phase by defining :

$$\Omega(s) = |\,\Omega(s)\,|\, e^{i\phi(s)} = \exp\left[\frac{s}{\pi}\int_{4m_\pi^2}^{\infty} ds'\,\frac{\phi(s')}{s'(s'-s)}\right] \qquad (11).$$

The dispersion relation for $\ln\Omega(s)$ has to be subtracted to converge and this subtraction

is conveniently made at $s = 0$. Eq. (11) corresponds to choosing $\Omega(0) = 1$. Such a relation as Eq. (11) exists for each partial wave amplitude. Unlike the amplitude $\mathcal{F}$, $\Omega(s)$ has only a right hand cut, but it is constructed so that $g_1 = \mathcal{F}(s)\Omega(s)^{-1}$ is real for $s \geq 4m_\pi^2$ and so g_1 has no right hand cut [30,31].

We can then write a dispersion relation for g_1 by integrating over its left hand cut. Let us first assume (wrongly) that this satisfies an unsubtracted dispersion relation, so [30]

$$\mathcal{F}(s) = \frac{\Omega(s)}{\pi} \int_{-\infty}^{0} ds' \frac{\mathrm{Im}\mathcal{H}(s')\,\Omega^{-1}(s')}{s' - s} \qquad (12).$$

This tells us that if we know $\Omega(s)$ everywhere and we know the discontinuity across the left hand cut (i.e. we know the details of all of π, ρ, ω, $\rho\rho$, $\omega\omega$, ... exchange), then we would know the $\gamma\gamma \to \pi\pi$ amplitude everywhere, Fig. 12. Indeed, this would mean that all resonances in $\gamma\gamma \to \pi\pi$ would have their couplings determined by the intricate details of the t and u-channel exchanges. While this is in fact true, it is not exactly useful, since it is only the nearby part of the left hand cut, generated by the Born amplitude, that the low energy theorem guarantees is known. If we were to approximate $\mathcal{H}$ by $\mathcal{B}$ in Eq. (12), then we would find that the resulting amplitude $\mathcal{F}$ would in fact have a zero at the first expected resonance in each partial wave. That is, for instance, for the $I = 0$ D-wave such an approximation with no t, u-channel exchanges than the pion would have an $f_2(1270)$ with no coupling to $\gamma\gamma \to \pi\pi$. Figs. 2,3,12, if not common sense, tell us that to determine resonance couplings one must know more than the details of the nearby left hand cut. However, if we just want to predict the low energy $\gamma\gamma \to \pi\pi$ cross-section (as we do here) then this is dominated by the nearby part of the left hand cut, which we know all about (Fig. 12). Embellishments like form-factors, Fig. 13c, or elementary ρ-exchange only change the discontinuity ($\mathrm{Im}\mathcal{H}$) for $s < -m_\rho^2$ (Fig. 12).

Thus, below 500 MeV each partial wave amplitude is expected to be well determined and the $\gamma\gamma \to \pi^+\pi^-$ cross-section predicted to a few percent or so. Calculation (see later) reveals that final state interactions enhance the naive Born cross-section below 350 MeV and depress it above. Refs. [32,33] show how these general principles do not permit the large enhancement indicated by the PLUTO and DM1/2 results. Moreover, this prediction is well confirmed [5] by the Mark II data, Fig. 2. In contrast, the $\gamma\gamma \to \pi^0\pi^0$ amplitude involves an exact cancellation of the nearby part of the left hand cut. Thus the prediction for this cross-section is much more sensitive to the more distant part of this cut (Fig. 12).

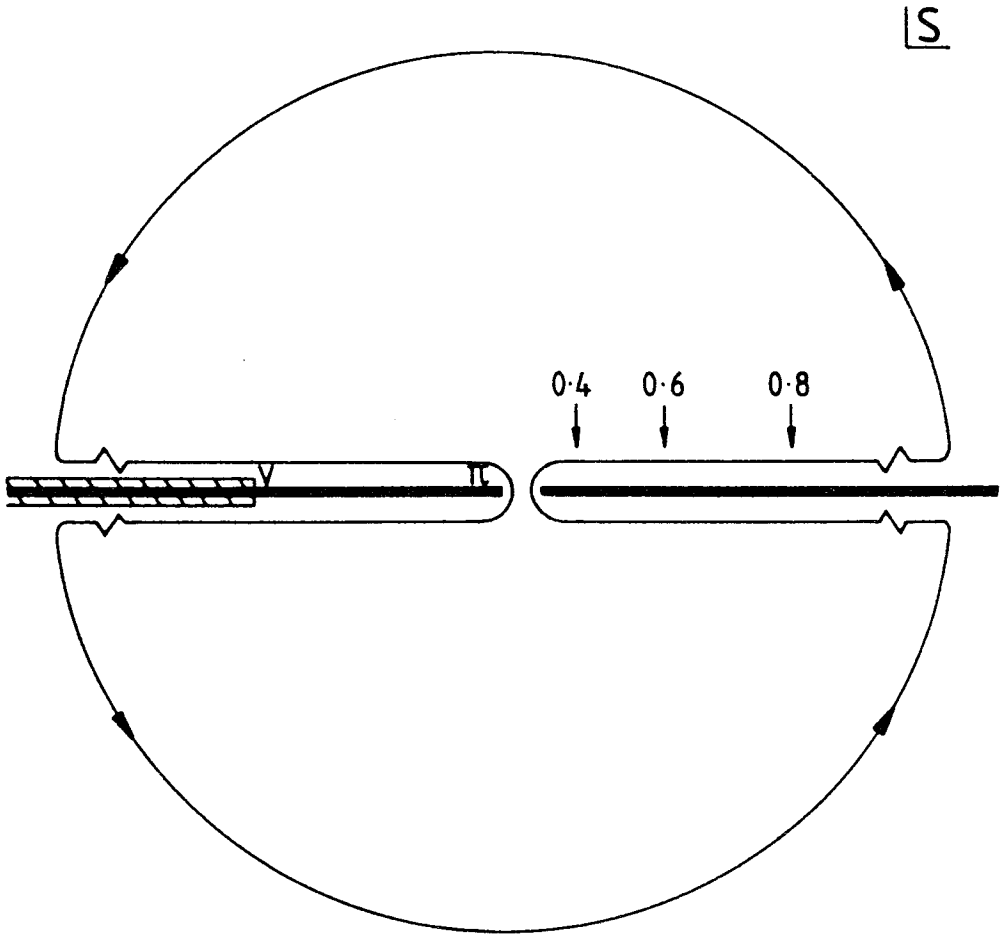

Fig. 12 : Complex s-plane for the partial wave amplitudes, $\mathcal{F}$, with a typical contour for a dispersive integral. The positions of the cuts are drawn to scale. The π and V show the start of the π and the vector exchange contributions to the left hand cut. The arrowed numbers along the right hand cut mark the c.m. energy in GeV.

To proceed to a detailed calculation of $\gamma\gamma \to \pi^0\pi^0$, let us note that the unsubtracted relation of Eq. (12) can be re-expressed in terms of a dispersive integral over the right hand cut (seen by considering a dispersion relation for $g_2 = (\mathcal{F} - \mathcal{H})\,\Omega^{-1}$) :

$$\mathcal{F}(s) = \mathcal{H}(s) - \frac{\Omega(s)}{\pi} \int_{4m_\pi^2}^{\infty} ds' \, \frac{\mathcal{H}(s')\,\mathrm{Im}\Omega^{-1}(s')}{s' - s} \qquad (13).$$

If no subtractions were indeed required the low energy theorem, Eq. (4), would automatically be ensured by the integral in Eq. (13) vanishing as $s \to 0$. However, subtractions are necessary and the fact that we have an exact low energy theorem makes this determinable. It is the form of Eq. (13) that illustrates how this works. We first write an unsubtracted relation for $g_3 = (\mathcal{F} - \mathcal{H})\,\Omega^{-1}/s$, which the low energy theorem ensures

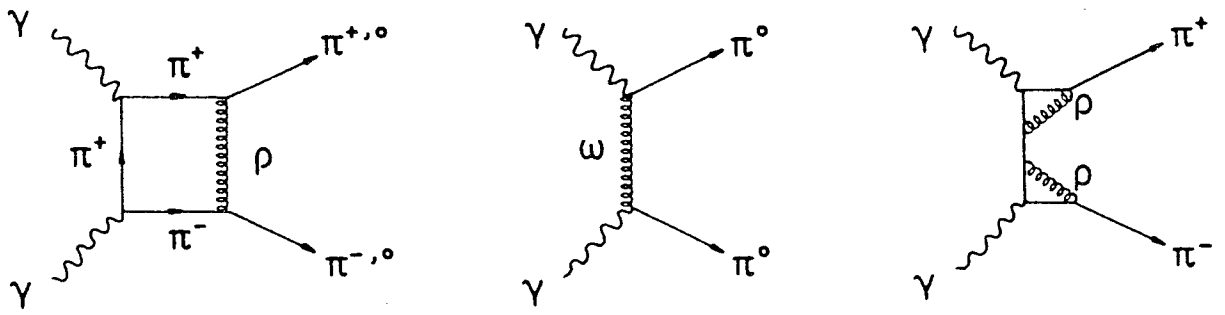

Fig. 13 : Examples of other than one-pion-t-channel exchange contributions to $\gamma\gamma \to \pi\pi$: (a) $\pi\rho$ exchange, (b) ω exchange, (c) form-factor effects.

is finite at $s = 0$. This gives :

$$\mathcal{F}(s) = \mathcal{H}(s) - \frac{s\Omega(s)}{\pi} \int_{4m_\pi^2}^{\infty} ds' \frac{\mathcal{H}(s')\,\mathrm{Im}\Omega^{-1}(s')}{s'(s'-s)} \qquad (14).$$

While the integral along the cut undoubtedly converges, the contour at infinity (Fig. 12) will only give a negligible contribution provided the difference $\mathcal{F}(s) - \mathcal{H}(s) \sim s^\gamma$ with $\gamma < 0.3$ for $I = 0$, since $| \Omega^{-1} | \sim s^{\phi(\infty)/\pi}$, where Regge considerations [4] give $\phi(\infty) \sim 121^o$. Thus a careful matching of the behaviour of the left hand cut amplitude to that of the full amplitude must occur, if this is to converge. We relegate to Appendix A the details of evaluating Eq. (14). Diagrammatically Eq. (14) with $\mathcal{H} = \mathcal{B}$ gives the contribution to $\gamma\gamma \to \pi^0\pi^0$ shown in Fig. 13a. This gives a low energy $\pi^0\pi^0$ cross-section of 30 nb or so, which is roughly in the right region — recall the $\pi^+\pi^-$ cross-section is 400 nb at low energies ! However, a detailed knowledge of the vector meson exchanges, Fig. 13b, is essential to get a more precise prediction and this is detail we do not really know. See Appendix A for a discussion of this.

Now one effect such contributions must have is to impose a PCAC zero in the $\gamma\gamma \to \pi^0\pi^0$ S-wave amplitude for $s = O(m_\pi^2)$, much as current conservation of QED imposes a zero at $s = 0$. This PCAC zero results from a fine cancellation of the small ω-exchange component (Fig. 13b) with the small π-exchange plus final state interaction term (Fig. 13a). One can eliminate the need to know the details of how such a cancellation actually occurs by the use of twice subtracted dispersion relations, as stressed by Maiani [23]. The details of the more distant left hand cut is traded for knowledge of the positions of the PCAC zeros. Moreover, having two subtractions highlights the *known* low energy contribution to the dispersion relations. Thus we write a subtracted dispersion relation for $g_3(s)$ for the $I = 0,2$ S-wave amplitudes, $\mathcal{F}^I(s)$;

the higher partial waves of both helicities satisfy unsubtracted dispersion relations when suitable threshold factors are divided out, as we have previously discussed [4].

Subtracting at $s = 0$ we have [34] :

$$\mathcal{F}^I(s) = \mathcal{H}^I(s) + d_I s\,\Omega^I(s) - \frac{s^2\Omega^I(s)}{\pi}\int_{4m_\pi^2}^{\infty} ds' \frac{\mathcal{H}^I(s')\,\mathrm{Im}(\Omega^I(s')^{-1})}{s'^2\,(s'-s)} \qquad (15).$$

In terms of these isospin amplitudes, the S-wave amplitudes for the physical processes $\gamma\gamma \to \pi^+\pi^-$ and $\gamma\gamma \to \pi^0\pi^0$ are, in an obvious notation,

$$\mathcal{F}^{+-} = \sqrt{\frac{2}{3}}\mathcal{F}^0 + \sqrt{\frac{1}{3}}\mathcal{F}^2 \;; \qquad \mathcal{F}^{00} = -\sqrt{\frac{1}{3}}\mathcal{F}^0 + \sqrt{\frac{2}{3}}\mathcal{F}^2 \qquad (16).$$

The $\mathcal{H}^I(s)$, having only left hand cuts, are given (not as incorrectly stated in Ref. [34]) by

$$\begin{aligned} \mathcal{H}^0(s) &= \sqrt{\frac{2}{3}}\mathcal{B}_\pi(s) - \mathcal{L}_\rho(s) - \sqrt{\frac{1}{3}}\mathcal{L}_\omega(s) \\ \mathcal{H}^2(s) &= \sqrt{\frac{1}{3}}\mathcal{B}_\pi(s) + \sqrt{\frac{2}{3}}\mathcal{L}_\omega(s) \end{aligned} \qquad (17)$$

so

$$\begin{aligned} \mathcal{H}^{+-}(s) &= \mathcal{B}_\pi(s) - \sqrt{\frac{2}{3}}\mathcal{L}_\rho(s) \\ \mathcal{H}^{00}(s) &= \sqrt{\frac{1}{3}}\mathcal{L}_\rho(s) + \mathcal{L}_\omega(s) \end{aligned}$$

where $\mathcal{L}_\rho$, $\mathcal{L}_\omega$ denote the contributions to the left-hand cut generated by exchanges with ρ and ω quantum numbers, respectively. Using Eq. (3), the cross-sections can then be deduced from these partial wave amplitudes.

According to Low's theorem

$$\mathcal{L}_\rho(s) \to 0 \quad , \quad \mathcal{L}_\omega(s) \to 0 \qquad \text{as } s \to 0 \,.$$

Recalling $\beta = \sqrt{1 - 4m_\pi^2/s}$ (Eq. (1)), the S-wave Born amplitude is [24,4]

$$\mathcal{B}_\pi(s) = \frac{1-\beta^2}{2\beta}\ln\left(\frac{1+\beta}{1-\beta}\right) \qquad (18)$$

with a cut for $s < 0$. Using Eq. (3), the cross-sections can then be deduced from these partial wave amplitudes. $\mathcal{L}_\rho$, $\mathcal{L}_\omega$ can be modelled explicitly by ρ and ω exchange [21]

to give

$$\mathcal{L}_V(s) = G_V \left[\frac{m_V^2}{\beta} \ln \left(\frac{1+\beta+s_V/s}{1-\beta+s_V/s} \right) - s \right] \tag{19}$$

where $s_V = 2(m_V^2 - m_\pi^2)$, with m_V the vector meson mass. $\mathcal{L}_V$ has a cut for $s < -(m_V^2 - m_\pi^2)^2/m_V^2$. The decay rate for $\omega \to \pi\gamma$ [35] fixes * $G_\omega = (1.34 \pm 0.10)$ GeV^{-2} and vector meson dominance suggests $G_\omega \gg G_\rho \simeq G_\omega/9$. Elementary vector meson exchange has a well-known fixed pole at $J = 0$ in the complex angular momentum plane [36]. Reggeization can be achieved by comparing the simple pole forms with their equivalent Veneziano amplitudes. Noting that for $|\, t \,|, |\, u \,| \leq m_V^2$

$$s \left[\frac{1}{m_V^2 - t} + \frac{1}{m_V^2 - u} \right] \simeq \frac{\Gamma(1-\alpha(t))\,\Gamma(1-\alpha(u))}{\Gamma(1-\alpha(t)-\alpha(u))}$$

where $\alpha(t) = \frac{1}{2} + (t - m_\pi^2)/s_V = 1 + (t - m_V^2)/s_V$. Then we can alternatively use

$$\mathcal{L}_V(s) = \frac{G_V m_V^2\, s}{2 s_V} \int_0^1 dz\, \mathrm{B}\left(\frac{1}{2} + \frac{s(1-\beta z)}{s_V}, \frac{1}{2} + \frac{s(1+\beta z)}{s_V} \right) \tag{20}$$

as the S-wave of a Reggeized amplitude, where $\mathrm{B}(a,b)$ is the usual beta-function. Note that the two forms of Eqs. (19,20) have quite different values for the subtraction constants d_I corresponding to different forms for $\mathcal{H}(s)$. Having different asymptotics, these two forms do not give exactly the same results when substituted in Eq. (15). The variation gives us an idea of the range of uncertainty in our calculations associated with high energy behaviour and a measure of the effect of more massive exchanges in the t and u-channels. This will be displayed in the plots of our results below.

This leaves just the two subtraction constants d_0, d_2 to be fixed by PCAC. For massless pions, the CAC conditions are imposed at $s = 0$. For physical mass pions, PCAC still sets $\mathcal{F}^{+-}(s) = \mathcal{B}(s) + O(s^2)$ as $s \to 0$, but for the $\pi^0\pi^0$ zero it requires that $\mathcal{F}^{00}(s) = 0$ only for $s \equiv s_n = O(m_\pi^2)$. Lowest order Chiral Perturbation Theory [18,19] places this zero on-shell at the same position as that for lowest order $\pi^+\pi^- \to \pi^0\pi^0$, namely at $s_n = m_\pi^2$. Though $\pi\pi$ data indicate this is roughly right [37,38], it would be too restrictive to impose this exactly. We shall thus just require $s_n = O(m_\pi^2)$ and show results accordingly.

---

* note that in [34] an incorrect comparison of the formulae of Refs. [24,4] with those of Ko [21] was made and so G_ω was there half as large as it should have been.

That lowest order Chiral Perturbation Theory puts the Adler zero in the $\gamma\gamma \to \pi^0\pi^0$ S-wave at the same position as that in the $\pi^+\pi^- \to \pi^0\pi^0$ is a consequence of the proportionality of $\mid \mathcal{F}(\gamma\gamma \to \pi^0\pi^0) \mid$ to $\mid \mathcal{T}(\pi^+\pi^- \to \pi^0\pi^0) \mid$ at all energies as noted by Donoghue et al. [19]. However, in general, this can only be true if the sole effect of final state interactions is to give the lowest order real $\gamma\gamma \to \pi\pi$ amplitudes phases, leaving their moduli still proportional. However, the calculations we present in sect. 3 show that these phases in turn enhance the modulus of the $I = 0$ amplitude (via $\mid \Omega^0 \mid$, Eq. (11)) by 60% at 400 MeV and decrease the $I = 2$ amplitude (via $\mid \Omega^2 \mid$) by 10%. The S-wave amplitude for $\pi^0\pi^0$ production in $\gamma\gamma$ reactions and in $\pi^+\pi^-$ scattering are then no longer simply proportional.

How a particle responds to external electromagnetic fields defines its polarizability. In external electric and magnetic fields an object has an induced dipole moment. These moments are proportional to the strength of the applied fields : the proportionality constants α, β define the object's electric and magnetic polarizability (β is not to be confused with the relativistic velocity in Eqs. (1,3,18-20)). This idea is familiar in nuclear physics, where static approximations apply. This concept has been generalized to relativistic particles in Ref. [39]. For the pion, α and β are related to the rate at which the $\gamma\pi \to \gamma\pi$ amplitude approaches its Born limit at threshold. Thus for the π^0, using the definition of Kaloshin and Serebryakov * [31] :

$$\begin{aligned}(\alpha - \beta)_{\pi^0} &= \frac{4e^2}{m_\pi} \lim_{s\to 0} \frac{\mathcal{F}^{00}(s)}{s} \\ &= \frac{4e^2}{m_\pi} \left[-\sqrt{\frac{1}{3}}\, d_0 + \sqrt{\frac{2}{3}}\, d_2 + \sqrt{\frac{1}{3}}\, \mathcal{L}'_\rho(0) + \mathcal{L}'_\omega(0) \right]\end{aligned} \tag{21}$$

where the result is expressed in fm^3, by convention. Thus the polarizability is determined by the subtraction constants and we tabulate the predictions for this quantity at the end.

* note that this definition is 4π larger than that used in [22].

3. Predictions for $\gamma\gamma \to \pi^0\pi^0$

In this section, we discuss the predictions obtained using the dispersion relation of Eq. (15) for the $I = 0, 2$ S-waves and Eq. (14) for the other waves on dividing out their threshold behaviour as detailed in [4]. To make these predictions we need to specify each of the following inputs :

IN1 : phases $\phi(s)$ to determine the Omnès function through Eq. (11) ;

IN2 : the left hand cut function $\mathcal{H}(s)$;

IN3 : the position of the Adler zero, s_n, in the $\gamma\gamma \to \pi^0\pi^0$ S-wave. We set $s_n = m_\pi^2$, unless otherwise stated.

3.i Weinberg phases

For orientation, we begin by inputting phases (**IN1**) predicted 25 years ago by Weinberg in his classic paper on $\pi\pi$ scattering [40]. In that model, the $I = 0, 2$ S-wave amplitudes in the neighbourhood of $\pi\pi$ threshold are given by forms which embody Adler zeros : –

$$t^0 = \frac{1}{16\pi f_\pi^2}\left(s - \frac{m_\pi^2}{2}\right) \quad , \quad t^2 = \frac{1}{16\pi f_\pi^2}\left(m_\pi^2 - \frac{s}{2}\right). \tag{22}$$

We assume these determine the low energy phases by identifying

$$t^I(s) = \sqrt{\frac{s}{s - 4m_\pi^2}}\,\delta^I(s) \tag{23}.$$

This gives the S-wave phases shown in Fig. 14, which are also those of lowest order Chiral Perturbation Theory [17,41]. In a channel with a large number (even an infinite) number of resonances, phase shifts increase indefinitely with energy, while the amplitude's phase, $\phi(s)$, does not, in general — indeed because of the onset of inelasticity, $|\,\phi\,| < \pi$. We therefore cut off the phases predicted by Eqs. (22,23) at the value they have reached by 800-1000 MeV, where inelasticity sets in. The predictions do not depend critically on the exact asymptotic phase.

For **IN2**, we first let $\mathcal{H} = \mathcal{B}$, i.e. the Born amplitude of Eq. (18) in Eq. (17). This gives the prediction shown in Fig. 15 labelled "π". We see it reproduces the results of lowest order Chiral Perturbation Theory for $\gamma\gamma \to \pi^0\pi^0$. However, since our formalism ensures unitarity by guaranteeing Eq. (10), the predicted cross-section does

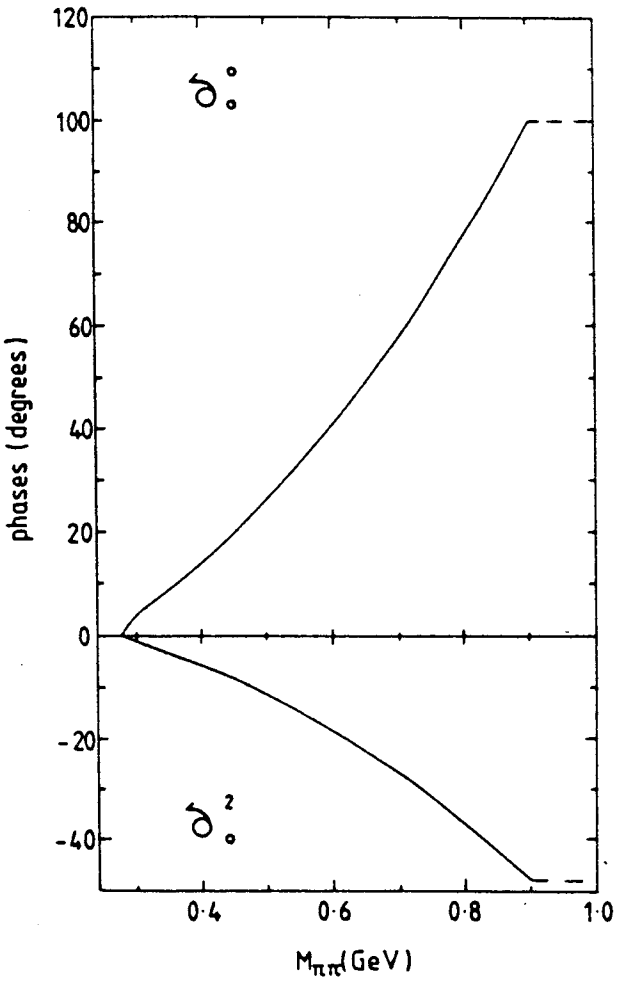

Fig. 14 : $I = 0, 2$ S-wave $\pi\pi$ phases as a function of invariant dipion mass, $M_{\pi\pi} = \sqrt{s}$ predicted by Eq. (23) from the Weinberg amplitudes of Eq. (22).

not continue to increase but slowly turns over. The corresponding polarizability, $(\alpha - \beta)$, of the π^0 defined by Eq. (21) is listed in Table I.

Next, we include in the left hand cut function, $\mathcal{H}$, not just π-exchange, but ρ, ω using either Eq. (19) or Eq. (20). These give the dashed curve in Fig. 15, which is hardly different from the solid curve below 400 MeV , and above looks rather like the results of Ko [21] and Bijnens et al. [20] of Fig. 6 (though a little lower), who compute similar dynamical effects. The shaded region illustrates the range given by using Eq. (19) or Eq. (20) for vector meson exchange.

These results show how our calculational scheme and the more specific one of given orders in Chiral Perturbation Theory are in excellent agreement. However, neither is in accord with the Crystal Ball data near threshold, where lowest order Chiral Perturbation Theory, being an expansion in powers of momentum is expected to work best.

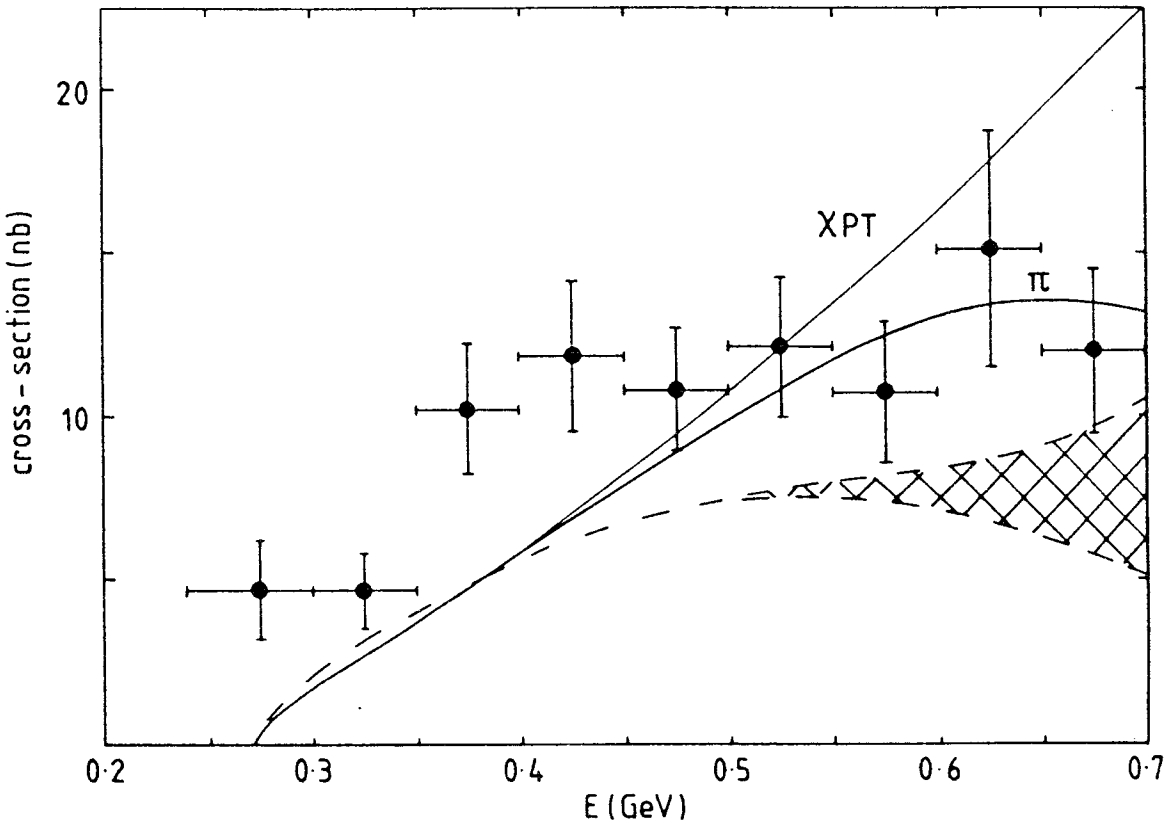

Fig. 15 : Integrated cross-section for $\gamma\gamma \to \pi^0\pi^0$ as a function of the $\pi\pi$ invariant mass, $E = \sqrt{s}$. The data are from Crystal Ball [3] scaled to the full angular range by a factor of 1.25. The line marked χPT is the prediction of lowest order Chiral Perturbation Theory [18,19]. The curve marked π is the dispersive calculation using Weinberg phases and just π-exchange for the left hand cut. The dashed curve includes ρ and ω exchange — the band delineates the range produced by different asymptotics for these vector exchanges.

So why this disagreement ? Let us start by comparing the input Weinberg phases with those measured in experiment, which come from two sources. The first is from a series of experiments on high energy dipion production by pion beams. At small momentum transfers such processes are dominated by pion exchange and by Chew-Low extrapolation [38] the physical $\pi\pi$ cross-section can be determined. The highest statistics experiments on both $\pi^+\pi^-$ and $\pi^+\pi^+$ production are by the CERN-Munich collaboration [42,43]. The S-wave $\pi\pi$ phases from several partial wave analyses of their data are shown in Fig. 16. A source of near threshold information is provided by studies of K_{e4} decays [44], which measure the interference of the S and P-waves, which by Watson's theorem allows the $I = 0$ $\pi\pi$ phase to be extracted [38]. While these agree with Weinberg phases very close to threshold, they very soon differ (Fig. 16).

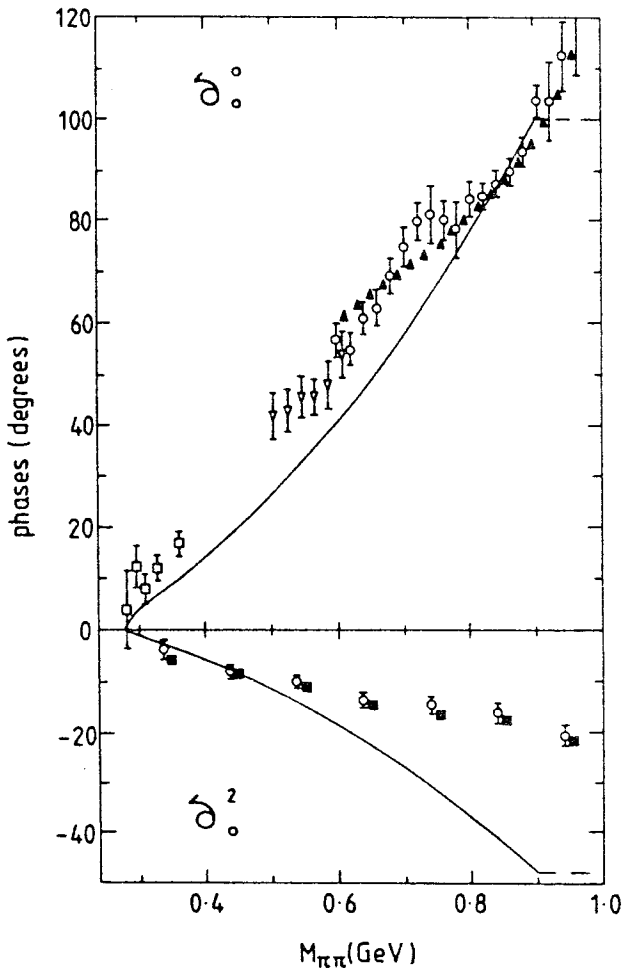

Fig. 16 : $I = 0$ and 2 S-wave $\pi\pi$ phase-shifts, δ_0^I, as a function of $\pi\pi$ mass, $M_{\pi\pi} = \sqrt{s}$. The data are described in the caption for Fig. 17. The curves are the extrapolation of the Weinberg predictions of Fig. 14.

3.ii Experimental $\pi\pi$ phases

Let us now for **IN1** input these experimental $\pi\pi$ phases. The analyses of the CERN-Munich experiments fix these above 500 MeV. Above $K\overline{K}$ threshold, we continue to choose the phase to be that of $\pi\pi \to \pi\pi$, where, of course, it need not be. However, as discussed in Refs. [4,27], this choice makes very little difference to the low energy prediction for $\gamma\gamma \to \pi\pi$. Here with twice subtracted dispersion relations, Eq. (15), the higher energy region is more strongly suppressed. Much more important is what is happening down towards threshold. There we have two constraints on the S-wave phases : the measurements inferred from K_{e4} decays [44], Fig. 17, and the constraints imposed by the Roy equations [45] that embody the analyticity and crossing of the $\pi\pi$ system. Study of these equations [46] teaches us that there is essentially a one

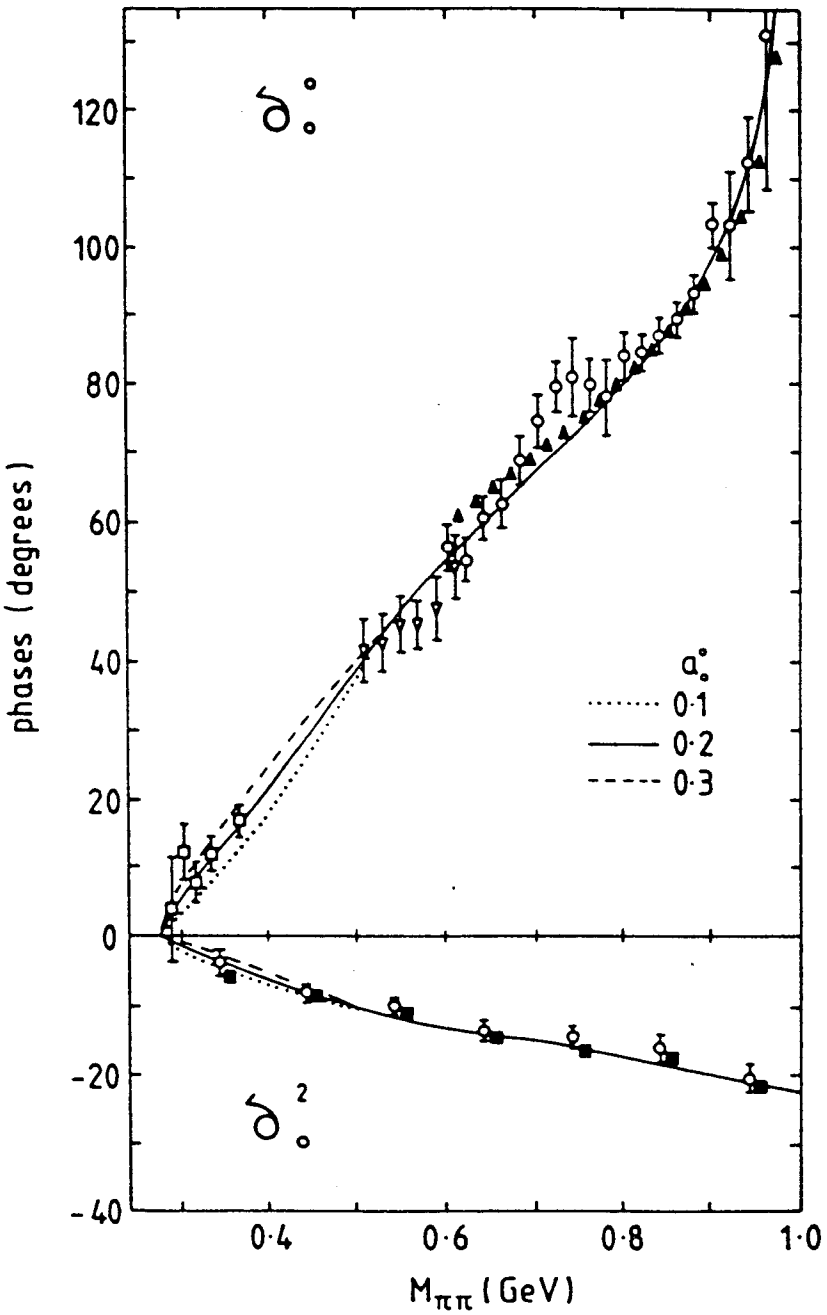

Fig. 17 : $I = 0$ and 2 S-wave $\pi\pi$ phase-shifts, δ_0^I, as a function of $\pi\pi$ mass, $M_{\pi\pi} = \sqrt{s}$. The data on δ_0^0 are from the K_{e4} experiment [44] (open squares), the rest are from different analyses of the CERN-Munich experiment [42]. The open triangles below 620 MeV are from the analysis of Estabrooks and Martin (averaging their s and t-channel treatments). Above 610 MeV are shown the results of the energy-independent (open circles) and energy-dependent (solid triangles) analyses of Ochs [42]. The I=2 phases, δ_0^2, in 100 MeV bins are the results of the two analyses of the data of Hoogland et al. [43] : method A (open circles), method B (solid squares). The solid line marks what are referred to as "central phases" and their extrapolation to threshold using the results of the study of the Roy equations with $a_0^0 = 0.2$, the dotted line has $a_0^0 = 0.1$ and the dashed line $a_0^0 = 0.3$.

parameter low energy extrapolation of the CERN-Munich phases for both the $I = 0$ and 2 S-waves. This parameter is naturally taken to be the $I = 0$ S-wave scattering length a_0^0, the Weinberg prediction [40], Eq. (22), for which is 0.15 for a pion decay constant of 93 MeV, or 0.20 in the Chiral Perturbation Theory treatment of Gasser and Leutwyler [17]. In Fig. 17 three such extrapolations with $a_0^0 = 0.1, 0.2, 0.3$ are shown.

In Figs. 18-21 are the resulting predictions for $\gamma\gamma \to \pi^0\pi^0$ integrated over the full angular range. Fig. 18 shows the prediction for a given $I = 0$ scattering length of 0.2 — the central line of Fig. 17. The curve marked "π" is with $\mathcal{H} = \mathcal{B}$ for **IN2**. The other curves include ρ, ω exchange ; the band illustrates the range according to whether Eq. (19) or (20) is used (as with Fig. 15). The experimental $I = 0$ phase is larger than what we call the Weinberg phase at low energies (Fig. 16) and this naturally leads to an increased $\gamma\gamma \to \pi^0\pi^0$ cross-section, but this is **not** because this cross-section is simply proportional to $\sin^2(\delta_0^0 - \delta_0^2)$ as it is in lowest order Chiral Perturbation Theory [19]. As discussed at the end of sect. 2, this is not the sum total of final state interactions. The moduli of the $I = 0$ and $I = 2$ amplitudes are, in fact, affected quite differently, being enhanced and suppressed, respectively, and it is this that is also responsible for the difference between the results of Figs. 15 and 18.

In Fig. 19 we fold in the sensitivity to changes in the $I = 0, 2$ S-wave phases above 520 MeV, which typically have errors [42,43] of $\pm\ 3^o$ and $\pm\ 2^o$ respectively (Fig. 17). The band delineates extremes. The upper (lower) boundary corresponds to increasing (decreasing) <u>all</u> the $I = 0$ phases by $3 - 4^o$ and decreasing (increasing) <u>all</u> the $I = 2$ phases by 2^o, simultaneously — bigger variations will be considered below. Fig. 20 shows the prediction with fixed phases above 520 MeV, but different Roy equation inspired extrapolations [46] of these down to threshold for $a_0^0 = 0.1$ to 0.3. Again the bands added to the highest and lowest a_0^0 predictions illustrate the effect of different treatments of ρ, ω exchanges. All the corresponding π^0 polarizabilities are given in Table I. Fig. 21 shows the result of varying **IN3** the Adler zero position from $s_n = m_\pi^2$, the results for which are bordered by the dotted lines, to $\frac{1}{2}m_\pi^2$ (the lower band) and $2m_\pi^2$ (the higher band). All three of these are for central CERN-Munich phases and $a_0^0 = 0.2$. As is clear from Figs. 8,12, the closer to $s = 0$ the Adler zero appears on-shell, the smaller the π^0's polarizability, $(\alpha - \beta)$ of Eq. (21), as seen in Table I.

Fig. 19 highlights how the use of $\pi\pi$ phases from experiment, rather than from low orders in Chiral Perturbation Theory, predicts a rather different $\gamma\gamma \to \pi^0\pi^0$ cross-section. Moreover, all the curves using experimental phases are reassuringly in general

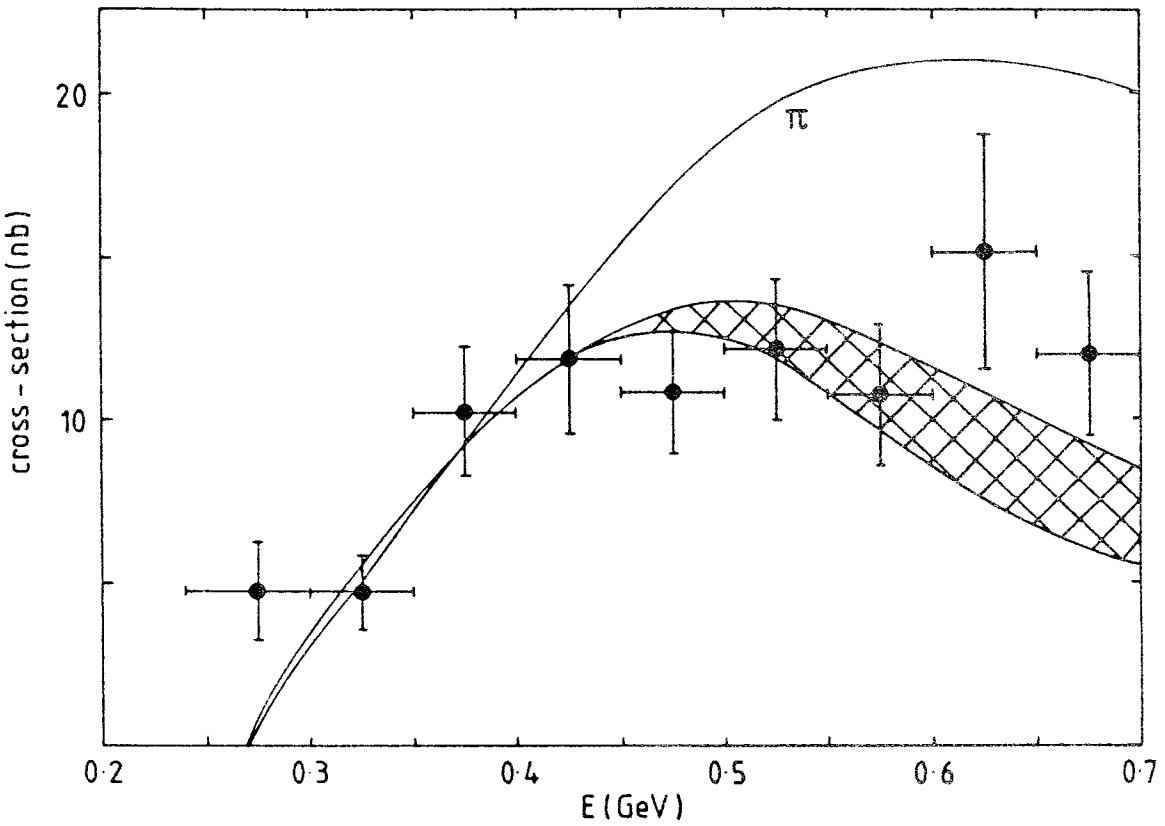

Fig. 18 : Integrated cross-section for $\gamma\gamma \to \pi^0\pi^0$ as a function of the $\pi\pi$ invariant mass, $E = \sqrt{s}$. The data are from Crystal Ball [3] scaled to the full angular range by a factor of 1.25. The curves depict our dispersive calculation using phases of Fig. 17 with $a_0^0 = 0.2$, that marked π uses just π-exchange for the left hand cut. The shaded region includes ρ and ω exchange — the band delineates the range produced by different asymptotics for these vector exchanges.

agreement with the Crystal Ball data, with a χ^2 of 1 per datum. Indeed, we see that precision data on $\gamma\gamma \to \pi^0\pi^0$ near threshold have the ability to pin down both the $\pi\pi$ scattering lengths (Fig. 20) as well as teach us about the on-shell appearance of the Adler zero in the $\gamma\gamma$ reaction (Fig. 21).

As a further test of the sensitivity to $\pi\pi$ phases, we present one last calculation. Schenk [47] has developed a parametrization of the experimental $\pi\pi$ phases that is designed to match on to the low energy predictions of Chiral Perturbation Theory [17]. The range of phases his parameters allow is illustrated by the curves in Fig. 22. We see they permit a larger variation than we considered before and they have a different extrapolation to threshold. Above 850 MeV, these parametrizations have been smoothly continued to our form of Fig. 17. These new phases give the $\pi^0\pi^0$ predictions of Fig. 23. The dashed lines delineate the range of possibilities and the shaded region the

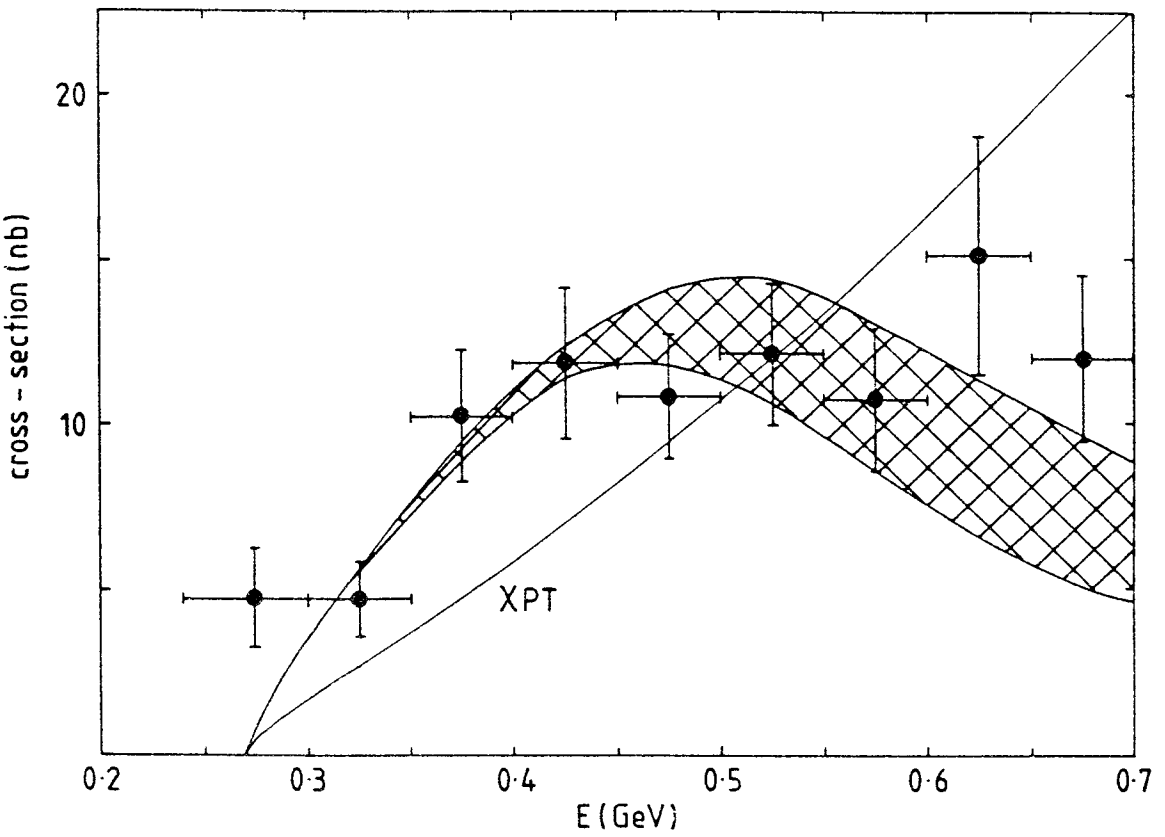

Fig. 19 : Integrated cross-section for $\gamma\gamma \to \pi^0\pi^0$ as a function of the $\pi\pi$ invariant mass, $E = \sqrt{s}$. The data are from Crystal Ball [3] scaled to the full angular range by a factor of 1.25. The band depicts our dispersive prediction using the central phases of Fig. 17 with $a_0^0 = 0.2$. The range, described in the text, is a reflection of both the experimental uncertainty above 500 MeV in the S-wave $\pi\pi$ phases shown in Fig. 17 and the different asymptotics for the vector exchanges. The line marked χPT is the prediction of lowest order Chiral Perturbation Theory [18,19].

prediction of the phases of curve 2 of Fig. 22. It will be seen that near threshold, these predictions of the Schenk phases do not rise as steeply as those of Figs. 18, 19, 21. Careful comparison of the curves through the phases of Figs. 17 and 22 reveals that the Schenk $I = 0$ phase, Fig. 22, does not rise quite as sharply between 300 and 400 MeV as those of Fig. 17, even though the scattering length is 0.2 for both the central line of Fig. 17 and of Fig. 22. Indeed, Schenk's rise is closer to the 0.1 curve of Fig. 17 and so, as indicated by the results of Fig. 20, predict a smaller $\pi^0\pi^0$ cross-section.

While such differences are immaterial for present data, one sees how precision measurements at DAΦNE may tighten up our knowledge of the $\pi\pi$ phases. Precise data on dipion production in both $\gamma\gamma$ reactions and K_{e4} decays would really pin these down. Such data would provide a particularly powerful constraint if both $\gamma\gamma \to \pi^0\pi^0$ and

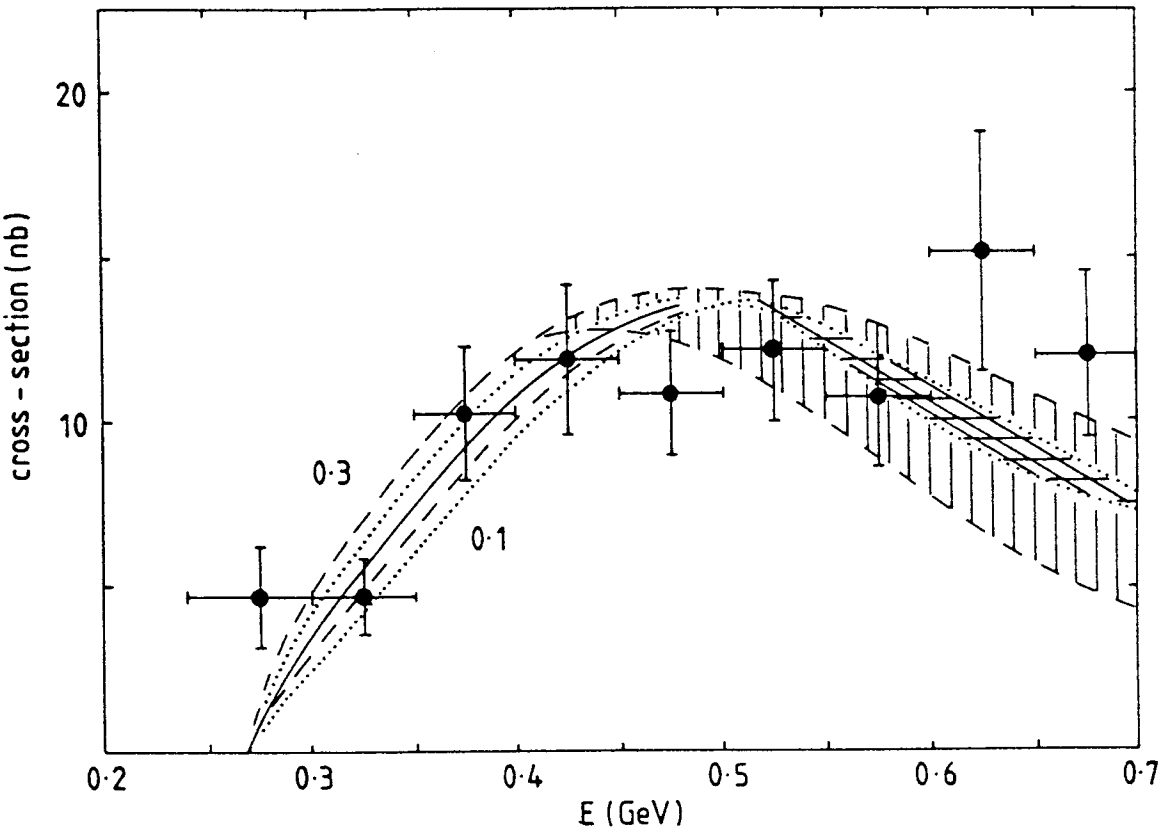

Fig. 20 : Integrated cross-section for $\gamma\gamma \to \pi^0\pi^0$ as a function of the $\pi\pi$ invariant mass, $E = \sqrt{s}$. The data are from Crystal Ball [3] scaled to the full angular range by a factor of 1.25. The lines, labelled by the value of the $I = 0$ $\pi\pi$ S-wave scattering length in steps of 0.05 from 0.1 to 0.3, illustrate the effect of different extrapolations of the central phases above 520 MeV (the solid line in Fig. 17) down to threshold on the dispersive prediction. The bands above 500 MeV on the $a_0^0 = 0.1$ and 0.3 curves mark the range generated by different asymptotics.

$\pi^+\pi^-$ were measured accurately. The prediction for these are closely correlated. In Fig. 24 is shown the dependence of the charged cross-section on the scattering length, a_0^0, as for Fig. 20. Note that here is shown the $\pi^+\pi^-$ cross-section integrated over the whole angular range. Experiment inevitably only covers a limited region and the expectation for that is not simply obtained by scaling from the full range. This is because for $\pi^+\pi^-$ production, as discussed in sect. 2, the cross-section is not dominated by its S-wave much above threshold. When experiments have been designed and set up [48], then will be the time to take their acceptance into account in these predictions.

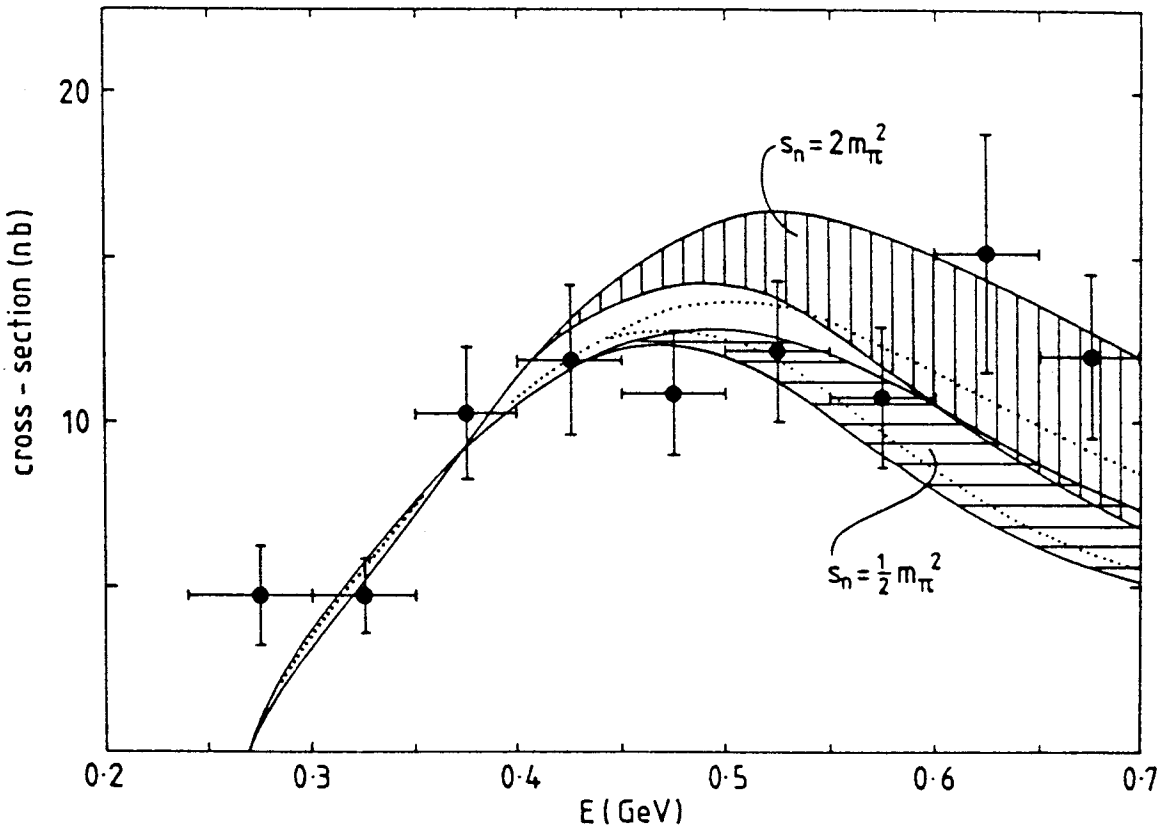

Fig. 21 : Integrated cross-section for $\gamma\gamma \to \pi^0\pi^0$ as a function of the $\pi\pi$ invariant mass, $E = \sqrt{s}$. The data are from Crystal Ball [3] scaled to the full angular range by a factor of 1.25. The three bands show the effect of varying the Adler zero for $\gamma\gamma \to \pi^0\pi^0$ from $s_n = \frac{1}{2}m_\pi^2$ (the lower, horizontally shaded region) to m_π^2 (the unshaded region bounded by the dotted lines) to $2m_\pi^2$ (the higher, vertically shaded region). Again the bands mark the uncertainties in the calculations.

4. Conclusion

What we have learnt from this analysis is that our general formalism based on dispersion relations, crossing and unitarity allows predictions to be made for low energy $\gamma\gamma \to \pi^+\pi^-$, $\pi^0\pi^0$ scattering with inputs from Chiral Perturbation Theory and from $\pi\pi$ experiments. Lowest order Chiral Perturbation Theory is found not to reproduce the Crystal Ball results on $\gamma\gamma \to \pi^0\pi^0$ — the only experiment that at present provides a normalized cross-section. Whilst Chiral Perturbation Theorists have regarded their finite calculation for this process as a gold-plated prediction, we have seen here that experiment teaches us that low orders in perturbation theory are not sufficient even at threshold. Higher orders are essential. This has lead to a variety of resummation techniques — both K-matrix approaches and Padé approximations have been advocated by Truong [49] to ensure Watson's theorem is fulfilled, or more recently a $1/N_f$ expansion

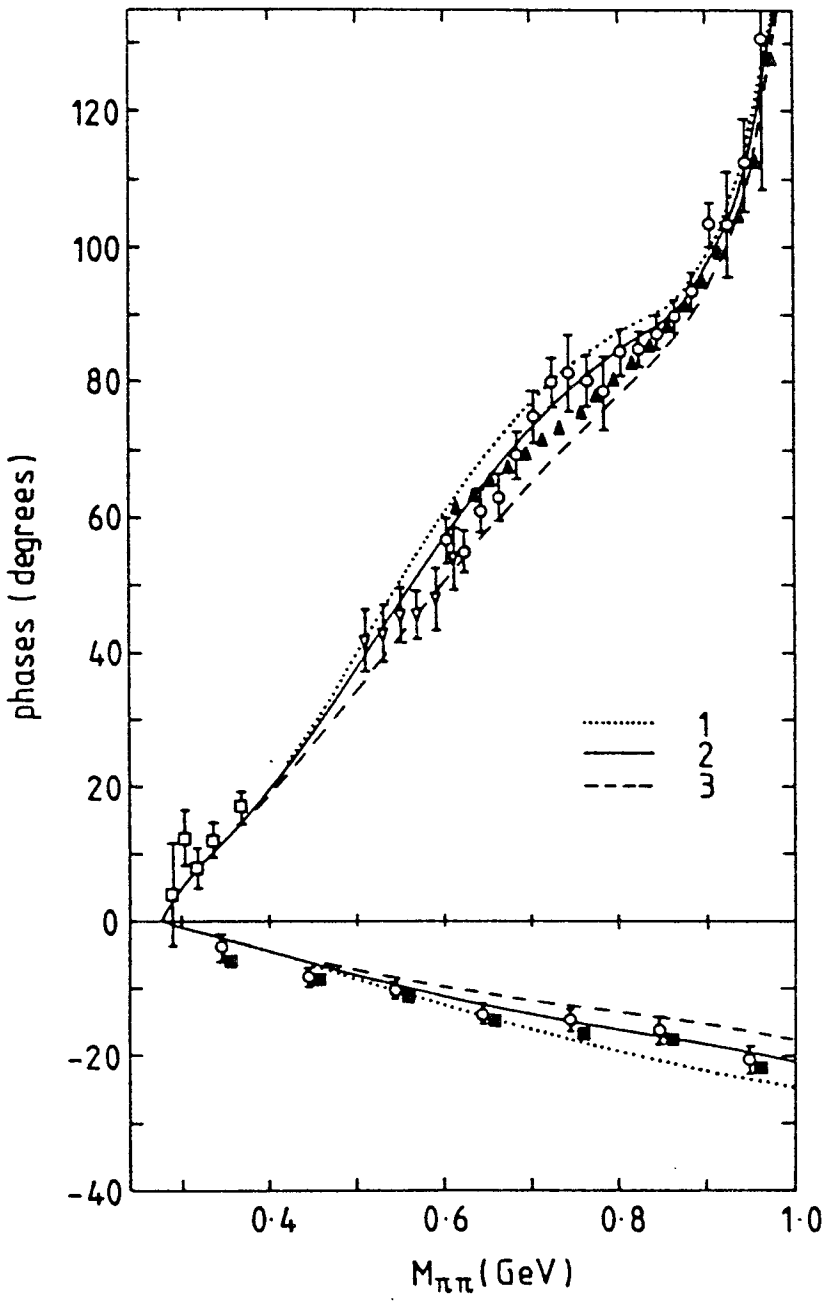

Fig. 22 : $I = 0$ and 2 S-wave $\pi\pi$ phase-shifts, δ_0^I, as a function of $\pi\pi$ mass, $M_{\pi\pi} = \sqrt{s}$. The data are as in Fig. 17. The curves marked 1,2, 3 are the phases given by the parametrizations A, B, C of Schenk [47], which continue towards threshold according to the predictions of Chiral Perturbation Theory [17,41].

by Im [50] — and hybrid approaches marrying perturbation theory with resonance physics by Goble, Rosenfeld and Rosner [51]. The surprise is that even at threshold, higher orders are important enhancing both the $\gamma\gamma \to \pi^0\pi^0$ cross-section and the π^0's polarizability by factors of two.

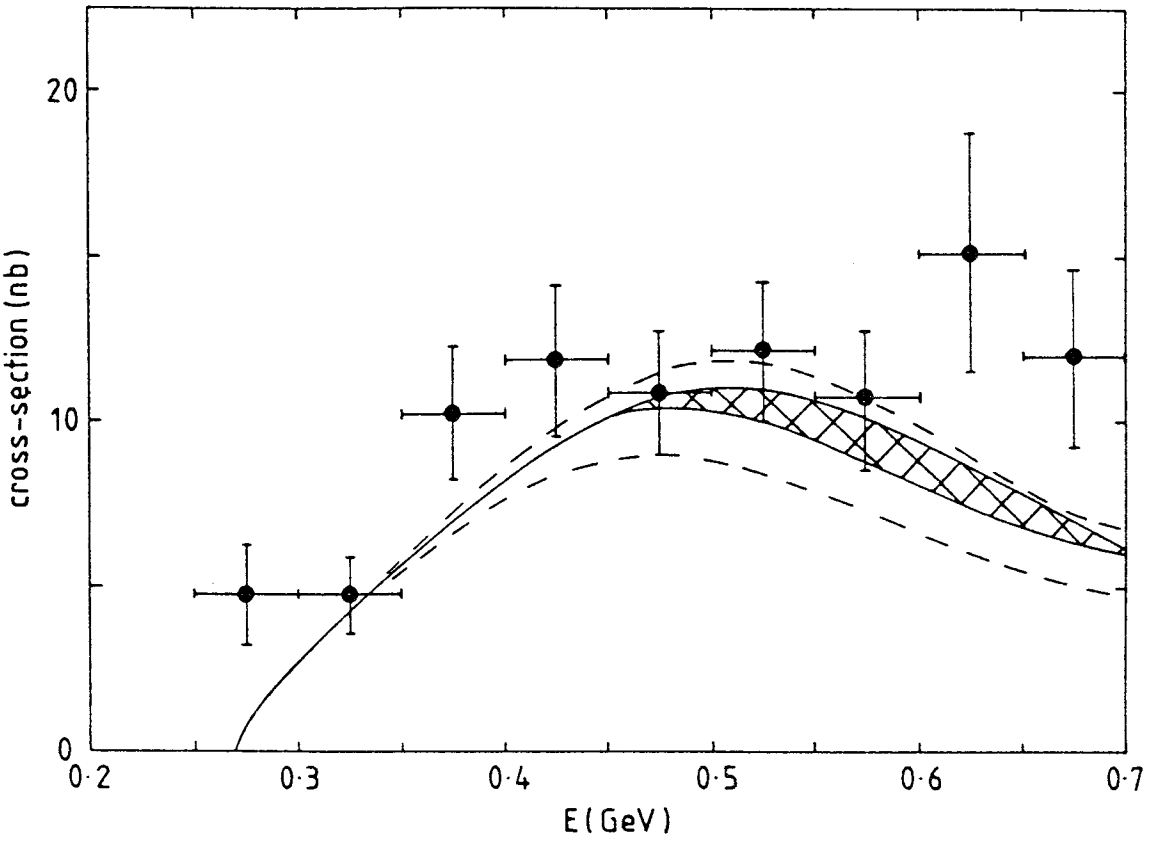

Fig. 23 : Integrated cross-section for $\gamma\gamma \to \pi^0\pi^0$ as a function of the $\pi\pi$ invariant mass, $E = \sqrt{s}$. The data are from Crystal Ball [3] scaled to the full angular range by a factor of 1.25. The curves depict our dispersive calculation using phases of Fig. 22. The shaded region is the result using the phases of curves 2 in Fig. 22. The dashed band marks the region allowed by phases between curves 1 and 3.

Low energy $\pi\pi$ interactions are weak — a consequence of the spontaneous breakdown of chiral symmetry. However, within a few hundred MeV of threshold these interactions become so strong that the unitarity constraint of Eq. (7) is only true non-perturbatively. While a perturbative expansion formally satisfies this constraint order by order, as soon as $| \mathcal{T} | \sim O(1)$, a non-perturbative approach is essential and that is what is automatically included in our formalism of sect. 2.

DAΦNE holds out the prospect of precision measurements of both charged and neutral dipion production in two photon reactions. Together with results on K_{e4} decays, these experiments will aid our understanding of how nature implements Chiral Dynamics. This will not only be useful in colouring in our picture of GeV physics, but, if the interactions of the weak gauge bosons become strong, will give us an important guide to what to expect at TeV scales.

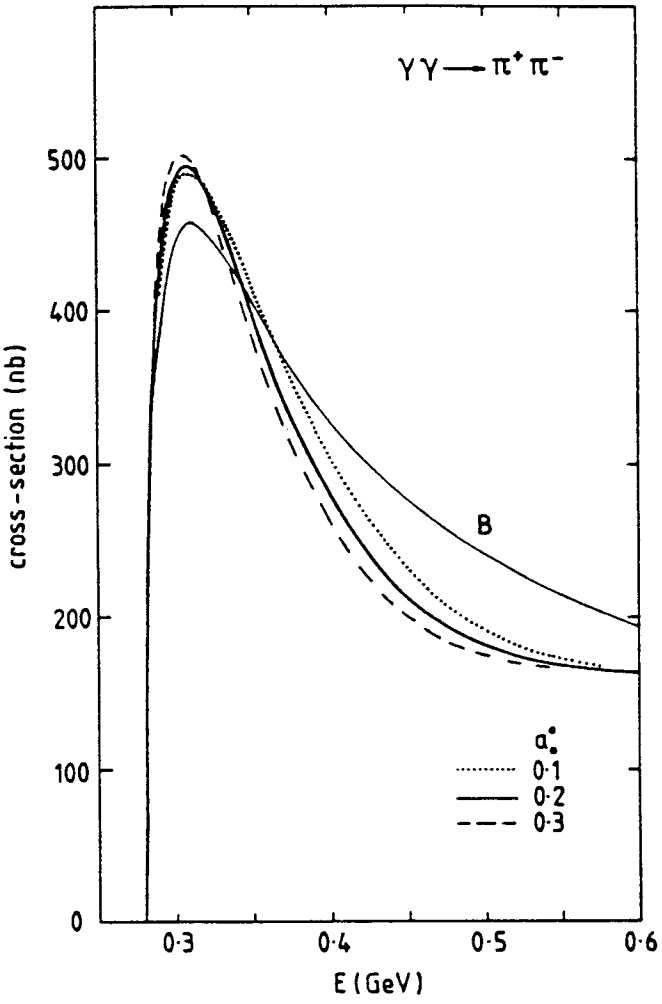

Fig. 24 : Dispersive predictions for the integrated cross-section for the $\gamma\gamma \to \pi^+\pi^-$ cross-section as a function of the $\pi\pi$ invariant mass, $E = \sqrt{s}$. The lines, labelled by the value of the $I = 0$ $\pi\pi$ S-wave scattering length in steps of 0.1 from 0.1 to 0.3, illustrate the effect of different extrapolations of the central phases above 520 MeV (the solid line in Fig. 17) down to threshold (cf. Fig. 20). The curve marked B is the Born cross-section given by the graphs of Fig. 9 [1,4,24].

Acknowledgements

It is a pleasure to thank David Morgan for a fruitful collaboration on the topic of $\gamma\gamma$ physics. I am most grateful to the members of the DAΦNE working group for their enthusiasm, especially to Stefano Bellucci, Juerg Gasser and Luciano Maiani for helpful and provocative discussions and to Rinaldo Baldini, Andre Courau and Paolo Franzini for focussing these on experimental realities.

Appendix A

In this Appendix, we discuss very briefly the difference in practice between the results using a once-subtracted dispersion relation, Eq. (14), and a twice subtracted relation, Eq. (15), for the S-wave amplitudes. As discussed in sect. 2, if the once subtracted relation converges, then in principle it will contain all the information about $\gamma\gamma \to \pi\pi$ scattering provided, of course, we know all the inputs into such a relation, $\mathcal{H}$ and Ω. As emphasised in sect. 2, the use of the twice subtracted relation, Eq. (15), obviates the need to know the behaviour of the distant left hand cut, particularly if one is interested in what happens in the low energy region for $\gamma\gamma$ scattering.

Let us assume that the once subtracted relation of Eq. (14) converges for both $I = 0$ and 2 S-wave amplitudes — higher waves cause no problem [4,5] so we do not discuss these in such detail. We will not enter here into the conditions for the vanishing of the contribution from the contour at infinity (Fig. 12), but suffice it say that the integral along the right hand cut in Eq. (14) does converge without difficulty. With the inputs of sect. 3, in particular the phases of Fig. 17, we evaluate the $\gamma\gamma$ amplitudes in the neighbourhood of threshold assuming just one-pion-exchange for the left hand cut, i.e. $\mathcal{H} = \mathcal{B}_\pi$. We use each of Eqs. (14, 15) and form the modulus of the charged and neutral pion amplitudes. These are plotted in Fig. 25. We see that the once subtracted dispersion relation gives a $\pi^0\pi^0$ amplitude below $\pi\pi$ threshold that is very small, compared to the charged one. Since we have only included the dominant one-pion-exchange component in the left hand cut of each isospin amplitude, the neutral S-wave does not know that the effect of the small contribution from all the non-pion exchanges is to enforce an Adler zero at $s_n = O(m_\pi^2)$. One sees from Fig. 25 how very tiny this contribution has to be — particularly compared with the full one pion exchange effect that occurs in the charged amplitude. The twice subtracted dispersion relation imposes the Adler conditions and we see gives $\gamma\gamma \to \pi\pi$ amplitudes that are not really very different on a global scale. Thus the predictions presented in Refs. [27,33] are in the same ball-park as the more detailed results, using twice subtracted dispersion relations and chiral symmetry, discussed here.

The polarizability of the pion is a useful measure when considering the low energy Compton scattering process, i.e. $\gamma\gamma \to \pi\pi$ as $s \to 0$, $t, u \to m_\pi^2$. As seen in Eq. (21), the quantity $(\alpha - \beta)$ for the π^0 is simply related to the slope of the amplitude, $\mathcal{F}^{00}(s)$, at $s = 0$. Fig. 25 highlights how this slope is not trivially related to what is happening in $\gamma\gamma \to \pi^0\pi^0$ for $s > 4m_\pi^2$. Consequently, great care must be taken in using oversimplified forms to infer the slope at $E = 0$ from the value of the cross-section for E between 300 and 500 MeV. Dispersion relations used here, of course, provide the ideal vehicle for such extrapolations.

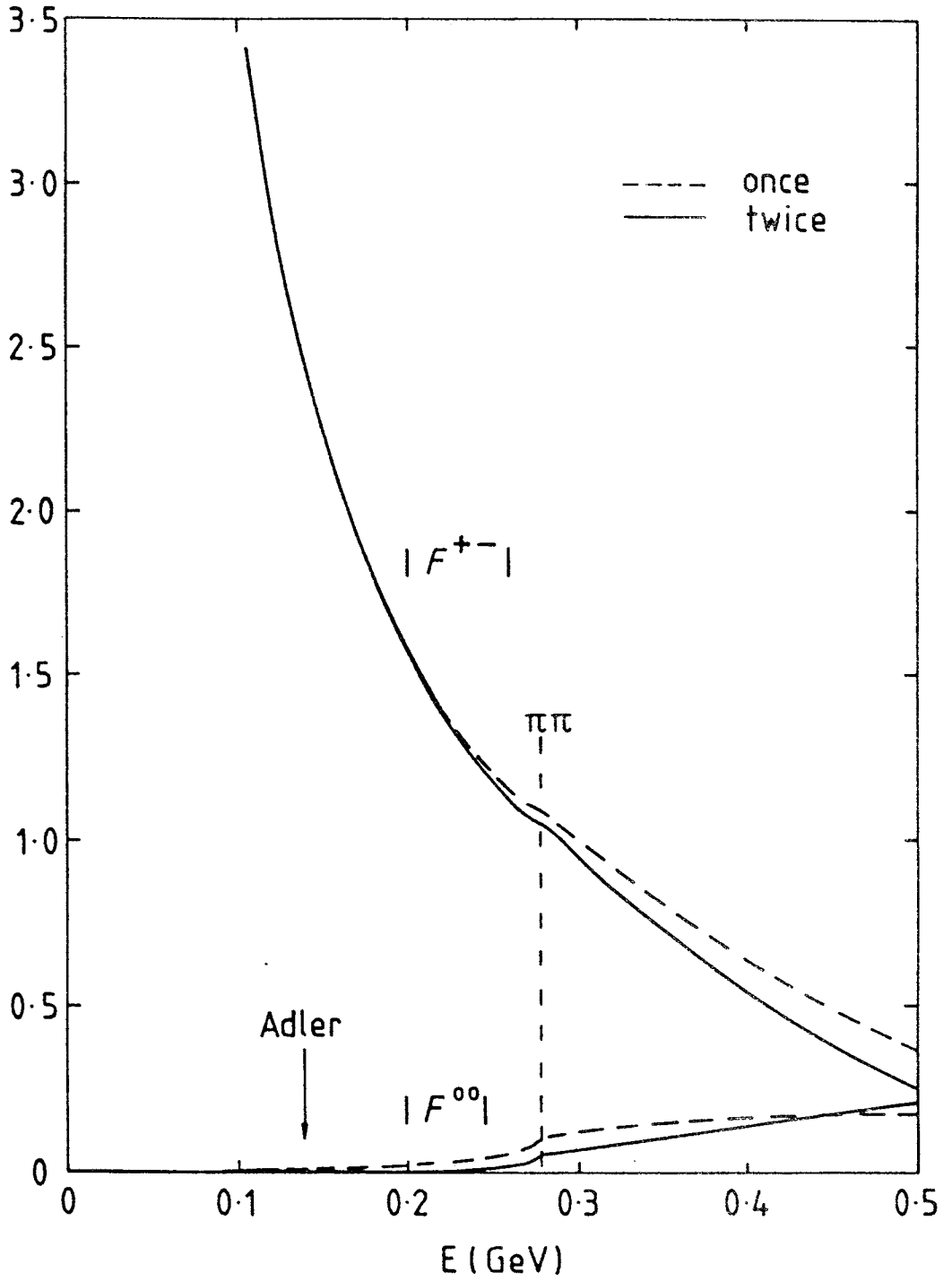

Fig. 25 : The modulus of the charged, $\mathcal{F}^{+-}$, and neutral, $\mathcal{F}^{00}$, dipion production S-wave amplitudes as functions of c.m. energy E. The solid (dashed) curves are the result of evaluating the twice subtracted dispersion relations, Eq. (15) (once subtracted Eq. (14)) with $\mathcal{H} = \mathcal{B}_\pi$ as input, together with the central phases of Fig. 17. The solid curve for $\mathcal{F}^{00}$ vanishes at $E = m_\pi$.

Phases IN1	**l.h. cut** IN2	s_n IN3	**π^0 Polarizability $(\alpha-\beta)$** $10^{-3}\,\mathrm{fm}^3$
Weinberg (Figs 14,16)	π	m_π^2	0.7
	π,ρ,ω	m_π^2	1.3 ± 0.1
phases (Fig. 17)			
$a_0^0 = 0.2$	π	m_π^2	0.9
$a_0^0 = 0.2$	π,ρ,ω	$\frac{1}{2}m_\pi^2$	0.7 ± 0.1
$a_0^0 = 0.2$	π,ρ,ω	m_π^2	1.5 ± 0.2
$a_0^0 = 0.2$	π,ρ,ω	$2m_\pi^2$	3.4 ± 0.3
$a_0^0 = 0.1$	π,ρ,ω	m_π^2	1.4 ± 0.2
$a_0^0 = 0.3$	π,ρ,ω	m_π^2	1.5 ± 0.2
phases 1,2,3 (Fig. 22)	π,ρ,ω	m_π^2	1.4 ± 0.2

Table I : π^0 Polarizability, $(\alpha-\beta)$ of Eq. (21), evaluated with different inputs **IN1-3.**

References

[1] S.J. Brodsky, T. Kinoshita and H. Terazawa, Phys. Rev. D4 (1971) 1532 ;
V.M. Budnev, I.F. Ginsburg, G.V. Meledin and V.G. Serbo, Phys. Rep. 15C (1975) 181 ;
Ch. Berger and W. Wagner, Phys. Rep. 146C (1987) 1 ;
H. Kolanoski and P. Zerwas in "High energy electron-positron physics", ed. A.Ali and P. Söding (World Scientific, 1988) ;
S. Cooper, Ann Rev. Nucl & Part. Phys. 38 (1988) 705.

[2] J. Boyer et al. (Mark II Collab.), Phys. Rev. D42 (1990) 1350.

[3] H. Marsiske et al. (Crystal Ball/DORIS Collab.), Phys. Rev. D41 (1990) 3324.

[4] D. Morgan and M.R. Pennington, Phys. Lett. 192B (1987) 207 , Z. Phys. C37 (1988) 431, Z. Phys. C39 (1988) 590.

[5] D. Morgan and M.R. Pennington, Z. Phys. C48 (1990) 623.

[6] T. Barnes, Proc. VII Int. Workshop on photon-photon collisions, Paris, 1986, ed. A. Courau ; Phys. Lett. 165B (1985) 434.

[7] N.N. Achasov and V.N. Ivanchenko, Nucl. Phys. B315 (1989) 465 ;
F.E. Close, Proc. Workshop on Physics and Detectors for DAΦNE, Frascati, April 1991, ed. G. Pancheri (INFN, Frascati) pp. 309-313.

[8] A. Courau et al. (DELCO Collab.), Phys. Lett. 147B (1982) 227.

[9] H. Aihara et al. (TPC/$\gamma\gamma$ Collab.), Phys. Rev. Lett. 57 (1986) 404.

[10] Ch. Berger et al. (PLUTO Collab.), Z. Phys. C26 (1984) 199.

[11] A. Courau et al. (DM1 Collab.), Nucl. Phys. B271 (1986) 1 ;
Z. Ajaltouni et al. (DM2 Collab.), Phys. Lett. B194 (1987) 573.

[12] C. Edwards et al. (Crystal Ball/SPEAR Collab.), Phys. Lett. 110B (1982) 82.

[13] J.H. Bienlein and K.-H. Karch, private communication.

[14] T. Oest et al. (JADE Collab.), Z. Phys. C47 (1990) 343.

[15] S. Adler, Phys. Rev. 137 (1965) B1022, Phys. Rev. 139 (1965) B1638.

[16] H. Pagels, Phys. Rep. 16 (1975) 221 ;
S. Weinberg, Physica 96*A* (1979) 327.

[17] J. Gasser and H. Leutwyler, Ann. Phys. (NY) 158 (1984) 142.

[18] J. Bijnens and F. Cornet, Nucl. Phys. B296 (1988) 557.

[19] J.F. Donoghue, B.R. Holstein and Y.C. Lin, Phys. Rev. D37 (1988) 2423.

[20] J. Bijnens, S. Dawson and G. Valencia, Phys. Rev. D44 (1991) 3555.

[21] P. Ko, Phys. Rev D41 (1990) 1531.

[22] S. Bellucci and D. Babusci, Proc. Workshop on Physics and Detectors for DAΦNE, Frascati (April 1991) ed. G. Pancheri (INFN, Frascati) pp. 351-360 ;
D. Babusci et al., ibid, pp. 383-392.

[23] L. Maiani, "Theory Working Group : Summary of Results", Proc. of Workshop on Physics and Detectors for DAΦNE, Frascati (April 1991) ed. G. Pancheri (INFN, Frascati) pp. 719-731.

[24] M. Poppe, Int. Journ. Mod. Phys. A1 (1986) 545.

[25] F.E. Low, Phys. Rev. 96 (1954) 1428 ;
M. Gell-Mann and M.L. Goldberger, Phys. Rev. 96 (1954) 1433.

[26] H.D.I. Abarbanel and M. Goldberger, Phys. Rev. 96 (1968) 1594.

[27] M.R. Pennington, Proc. VIII International Workshop on photon-photon collisions, Shoresh, Israel, 1988, ed. U. Karshon (World Scientific, 1988) pp. 297-325 ;
M.R. Pennington, Proc. of Workshop on Physics and Detectors for DAΦNE, Frascati (April 1991,) ed. G. Pancheri (INFN, Frascati) pp. 361-371.

[28] K.M. Watson, Phys. Rev. 88 (1952) 1163.

[29] R. Omnès , Nuovo Cim. 8 (1958) 316.

[30] D.H. Lyth, Nucl. Phys. B30 (1971) 195, Nucl. Phys. B48 (1972) 537; J. Phys. G10 (1984) 39, J. Phys. G10 (1984) 1777.

[31] A.E. Kaloshin and V.V. Serebryakov, Z.Phys. C32 (1986) 279.

[32] G. Mennessier and T.N. Truong, Phys. Lett. 177B (1986) 195.

[33] D. Morgan and M.R. Pennington, Phys. Lett. 192B (1987) 207.

[34] D. Morgan and M.R. Pennington, Phys. Lett. B272 (1991) 134.

[35] J.J. Hernandez et al. (Particle Data Group), Phys. Lett B239 (1990) 1.

[36] P.D.B. Collins, "An introduction to Regge theory and high energy physics", (Cambridge Univ. Press) Chap. 12.4.

[37] M.R. Pennington, "Zeros in $\pi\pi$ scattering", AIP Conf. Proc. No. 13 (PF Subseries No. 5), ed. P.K. Williams and V. Hagopian (AIP, NY, 1973) pp. 89-116.

[38] B.R. Martin, D. Morgan and G. Shaw, "Pion-pion Interactions in Particle Physics", (Academic Press, New York, 1976).

[39] I. Guiaşu and E.E. Radescu, Ann. Phys. (NY) 120 (1979) 145.

[40] S. Weinberg, Phys. Rev. Lett. 17 (1966) 616.

[41] J.F. Donoghue, C. Ramirez and G. Valencia, Phys. Rev. D38 (1988) 2195.

[42] W. Ochs, Univ. of Munich thesis, 1974 ;
P. Estabrooks and A.D. Martin, Nucl. Phys. B79 (1974) 301 ;
G. Grayer et al., Nucl. Phys. B75 (1974) 189 ;
H. Becker et al., Nucl. Phys. B151 (1979) 46.

[43] W. Hoogland et al., Nucl. Phys. B126 (1977) 109.

[44] L. Rosselet et al., Phys. Rev. D15 (1977) 574.

[45] S.M. Roy, Phys. Lett. 36B (1971) 353.

[46] J.L. Basdevant, C.D. Froggatt and J.L. Petersen, Nucl. Phys. B72 (1974) 413.

[47] A. Schenk, Nucl. Phys. B363 (1991) 97.

[48] A. Courau, Proc. Workshop on Physics and Detectors for DAΦNE, Frascati (April 1991) ed. G. Pancheri (INFN, Frascati) pp. 373-381.

[49] T.N. Truong, Phys. Rev. Lett. 61 (1988) 2526.

[50] C.J.C. Im, SLAC-Pub-5627 (Sept., 1991).

[51] R.L. Goble, R. Rosenfeld and J. Rosner, Phys. Rev. D39 (1989) 3264.